Efficacy of epicardial implantation of acellular chitosan hydrogels in ischemic and nonischemic heart failure: impact of the acetylation degree of chitosan

Orianne Domengé, Hélène Ragot, Robin Deloux, Agnès Crépet, Gaëlle Revet, Solène Emmanuelle Boitard, Alexandre Simon, Nathalie Mougenot, Laurent David, Thierry Delair, et al.

Efficacy of epicardial implantation of acellular chitosan hydrogels in ischemic and nonischemic heart failure: impact of the acetylation degree of chitosan

Orianne Domengé[1*], Hélène Ragot[2*], Robin Deloux[2*], Agnès Crépet[1], Gaëlle Revet[2], Solène Emmanuelle Boitard[2], Alexandre Simon[2], Nathalie Mougenot[3], Laurent David[1], Thierry Delair[1], Alexandra Montembault[1#], Onnik Agbulut[2#]

[1] Université de Lyon, Université Claude Bernard Lyon 1, CNRS, Ingénierie des Matériaux Polymères, IMP UMR 5223, 15 bd A. Latarjet, F-69622, Villeurbanne, France.

[2] Sorbonne Université, Institut de Biologie Paris-Seine (IBPS), CNRS UMR 8256, Inserm ERL U1164, Biological Adaptation and Ageing, 7 quai St-Bernard (case 256), F-75005, Paris, France.

[3] Sorbonne Université, UMS28 Plateforme d'Expérimentation Cœur, Muscles, Vaisseaux, 91 Bd de l'Hôpital, F-75013, Paris, France.

[*] These authors contributed equally.

[#] These authors jointly supervised this work and contributed equally.

Corresponding authors:

Prof. Onnik Agbulut, Sorbonne Université, Institut de Biologie Paris-Seine, UMR CNRS 8256, Inserm ERL U1164, 7, quai St Bernard (case 256), F-75005 Paris-France. Email: onnik.agbulut@sorbonne-universite.fr

Dr. Alexandra Montembault, Université Claude Bernard Lyon 1, CNRS, Ingénierie des Matériaux Polymères, IMP UMR 5223, 15 bd A. Latarjet, F-69622, Villeurbanne-France. Email: alexandra.montembault@recherche.univ-lyon1.fr

Abstract

This work explores the epicardial implantation of acellular chitosan hydrogels in two murine models of cardiomyopathy, focusing on their potential to restore the functional capacity of the heart. Different chitosan hydrogels were generated using polymers of four degrees of acetylation, ranging from 2.5% to 38%, because the degree of acetylation affects their degradation and biological activity. The hydrogels were adjusted to a 3% final polymer concentration. After complete macromolecular characterization of the chitosans and study of the mechanical properties of the resulting hydrogels, they were sutured onto the surface of the myocardium, first in rat after four-weeks of coronary ligation (n=58) then in mice with cardiomyopathy induced by a cardiac-specific invalidation of serum response factor (n=20). The implantation of the hydrogels was associated with a reversion of cardiac function loss with maximal effects for the acetylation degree of 24%. The extent of fibrosis, the cardiomyocyte length-to-width ratio, as well as the genes involved in fibrosis and stress were repressed after implantation. Our study demonstrated the beneficial effects of chitosan hydrogels, particularly with polymers of high degrees of acetylation, on cardiac remodeling in two cardiomyopathy models. Our findings indicate they have great potential as a reliable therapeutic approach to heart failure.

Keywords

Hydrogel; Natural Polymers; Cardiac Patch; Biocompatibility; Epicardial implantation; Heart failure; Dilated cardiomyopathy; Myocardial infarction.

1. Introduction

Heart failure is a progressive and life-threatening disease characterized by reduced systolic function as a consequence of cell death and by diastolic dysfunction due to increased fibrosis and reduced ventricular compliance [1]. Although ischemic cardiomyopathy induced by myocardial infarction (MI) is the most common cause of heart failure worldwide [2], nonischemic cardiomyopathy also significantly contributes to the number of patients with heart failure. In contrast to ischemic cardiomyopathies, which are amenable to a variety of pharmacological, electrical, and interventional treatments, the nonischemic forms of heart failure can only be treated symptomatically by drugs.

In the last few decades, engineered cardiac tissue scaffolds or cardiac patches have emerged as therapeutic candidates to substitute for damaged cardiac tissues as well as deliver regenerative factors after their epicardial implantation [3–5]. Cardiac patches were first investigated as a possible solution to cell injection challenges for cell therapy purposes [6]. Indeed, cell retention in damaged hearts appears to be one of the major roadblocks to successful myocardial regeneration in stem cell therapy. In this context, many studies demonstrated that the use of biomaterials for delivery and support of transplanted cells can provide a real solution to this obstacle [7–9]. In addition, cardiac patches can provide mechanical support to injured cardiac tissue to reduce adverse post myocardial infarction remodeling. In this perspective, in addition to cellularized cardiac patches, acellular cardiac patches have been developed from a variety of materials to provide structural support for the damaged ventricle, stimulate cellular recruitment into the material, and/or induce adaptive tissue remodeling and endogenous repair mechanisms [10,11]. Some authors have also demonstrated that acellular cardiac patches minimize inflammatory reactions after implantation by inducing the polarization of pro-inflammatory M1 macrophages into a pro-reparative M2 phenotype [12]. Epicardial implantation of acellular patches has been extensively explored across a number of clinically relevant animal models of ischemic injury, which demonstrated overall that surgically implanted patches can attenuate infarct expansion and left ventricular (LV) remodeling [13–16].

Numerous strategies have been proposed, including 3D-bioprinted scaffolds, electrospun scaffolds, decellularized tissues and various types of hydrogels to optimize the patches for cardiac regeneration [4,17,18]. Hydrogels are promising candidates in regenerative medicine because they are composed of hydrophilic polymer networks that can mimic specific physical aspects of the tissue microenvironments and extracellular matrix [19–21]. Chitosan-based hydrogels have been widely studied for biomedical applications, especially for myocardial applications [22]. Chitosan exhibits many key properties such as biodegradability [23], immune-promoting activities [24–26], antimicrobial activity [27,28] and wound-healing acceleration [29,30]. In this work, it is expected that chitosan promotes the regeneration process of the heart muscle and resorbs concomitantly leaving place to the neo-tissue that forms. This polysaccharide is industrially produced from the N-deacetylation of chitin in alkaline conditions [31,32]. Chitin is mainly extracted from the cuticles of

arthropods, the endoskeletons of cephalopods and the cell wall of fungi. Chitosan, as chitin, belongs to the family of linear copolymers of 2-amino-2-deoxy-D-glucose residues (glucosamine unit) and 2-acetamido-2-deoxy-D-glucose residue (acetyl-glucosamine unit) linked by β (1→4) glycosidic bonds. The degree of acetylation (DA) of these polymers is defined as the molar fraction of acetyl-glucosamine units. The name "chitosan" refers to polymers soluble in dilute acidic solutions, and then to DAs below 70% when the structure is that of a statistical copolymer [33]. As a general trend, the DA impacts the physico-chemical [34,35] and mechanical [36] but also the biological properties of chitosans [37].

The physical gelation of chitosan is widely reported in the literature [36,38–40]. Our previous work described the design of physical hydrogel patches composed only of water and chitosan of low DA, and their implantation onto the surface of the cardiac muscle in order to regenerate the infarcted myocardium [41]. These physical chitosan hydrogels have the advantage of being cross-linker-free and stable in physiological medium. Such chitosan hydrogels were prepared by varying two parameters: the polymer concentration and the gelling agent (gelation under ammonia vapors [36] or by contact with a NaOH aqueous solution [42]). This work pointed out that the most adapted chitosan concentration was approximately 3% (w/w (equivalent to g/g)) and that the mechanical properties of chitosan hydrogels prepared with aqueous NaOH solution were more suitable for cardiac implantation than those of hydrogels prepared using ammonia vapors. Biologically, patches produced by neutralization of chitosan solution with NaOH were perfectly incorporated onto the epicardial surface of the heart but the cell invasion into the patches was low [41]. Nevertheless, previous works have shown that the cell invasion within chitosan hydrogels obtained from the same gelation process may be promoted with an increase in the DA of chitosan [37,42].

In this context, the goal of the present study was to develop a hydrogel patch that would be better integrated in contact with the cardiac tissue. For this purpose, the influence of the DA of chitosan on the biological properties of the patches was investigated. Thus, we generated physical chitosan hydrogels by a NaOH induced-gelation process, using chitosan with DAs ranging from 2.5% to 38%, while having the same final polymer concentration (~ 3% (w/w)). The mechanical properties of the hydrogel patches were then studied before their implantation. We chose to work with chitosans with a relatively high molar mass (Mw). The mechanical properties of chitosan hydrogels prepared from polymers with high Mw are generally higher. Finally, the potential benefit of epicardial implantation of chitosan hydrogels with different DAs was evaluated in a murine model of both ischemic and nonischemic cardiomyopathies, focusing particularly on their potential to restore the functional capacity of the heart.

2. Material and Methods

2.1. Purification, acetylation and characterization of chitosan

The chitosan used in this study was produced from the N-deacetylation of chitin extracted from squid pens (calamari endoskeletons) and was purchased from Mahtani Chitosan (batch type 114). Before use, the polymer was purified as follows. The chitosan was dissolved at 0.5% (w/w) in an aqueous solution of acetic acid. The amount of acetic acid was added in stoichiometric amounts with the NH_2 sites of the chitosan. The resulting solution was filtered successively through 1.2, 0.8 and 0.45 µm membranes (Millipore) and then the chitosan was precipitated by the addition of ammonium hydroxide solution (29% (w/w)) until a pH of 9 was reached. The chitosan was thoroughly washed with deionized water and freeze-dried.

The N-acetylation of chitosan was obtained in a water/1,2-propanediol mixture with acetic anhydride as the reagent [39]. Briefly, an aqueous acetic acid solution of chitosan was prepared at a concentration of 1% (w/w) (chitosan was dissolved in deionized water containing the amount of acid necessary to achieve the protonation of the NH_2 sites). Then, 1,2-propanediol was added to obtain a final polymer concentration of 0.5% (w/w). A solution of acetic anhydride was slowly added to this hydroalcoholic solution under strong stirring. The amount of acetic anhydride corresponded to the stoichiometric amount necessary to achieve a given degree of acetylation of chitosan (in this study, 12%, 24% or 38%). The medium was left to stand for 12 h. We afterwards precipitated the final chitosan with aqueous ammonia (29% (w/w)). Finally, the polymer was washed in deionized water and freeze-dried as previously described [40].

After freeze-drying, ^{1}H NMR analysis was used to precisely determine (±5%) the degree of acetylation (DA) of each chitosan [43]. This spectral analysis also allowed us to check the absence of 1,2-propanediol in the reacetylated chitosans. We dissolved the polymer (15 mg) in 1 g of D_2O containing 5 µL of HCl overnight, and the spectrum was acquired at 25 ± 1°C by using a spectrometer Bruker Avance III 400 MHz 5 mm (ν=400 MHz). The DA was then calculated by the method of Hirai *et al.* [43]. As proposed by these authors in their publication, the DA was deduced from the ratio of the integrated area of the methyl protons peak of the N-acetyl glucosamine residues to that of all the H2 to H6' protons of both glucosamine and N-acetyl glucosamine residues (see an example of ^{1}H NMR spectrum in Figure S2).

The weight-average molecular weight (Mw) and dispersity (Đ) of the different chitosans were determined using size exclusion chromatography (SEC) coupled online with a differential refractometer (Optilab T-rEX, Wyatt; λ=658 nm) and with a multiangle laser light scattering (MALS) detector (Dawn-HELOES II, Wyatt; λ=664 nm). Thus, the polymer was dissolved in 0.15 mol.L^{-1} ammonium acetate/0.20 mol.L^{-1} acetic buffer (pH 4.8); the solution was then filtered through a 0.45 µm Millipore membrane, injected (v=100 µL) and eluted at a flow rate of 0.5 mL.min^{-1} (1260 Infinity

pump, Agilent Technologies) through two columns, TSK G2500 PW and TSK G6000 PW. As the sample passes through the steric exclusion chromatography columns, it is separated into fractions according to different hydrodynamic volumes. The online refraction index measurement allows us to determine the amount of each fraction. The online multi-angle light scattering allows us to determine the molar masses of each fraction. In order to perform measurements without calibrant samples, the refractive index increments (dn / dC) have been determined in a previous study [34]. The water content of the freeze-dried chitosan samples was evaluated using a thermogravimetric analyzer (DuPont Instrument 2950 thermogravimetric analyzer) operating at a temperature ramp of 10°C.min^{-1}, from 25°C to 250°C, under a flow of helium.

The full molecular characteristics of the different prepared chitosan samples are given in **Table 1**.

Table 1. Characteristics of the different chitosan samples used in this work.

DA (%)	Water content (%) (w/w)	Mw (g.mol^{-1})	Đ	DPw
2.5 ± 0.1	7.6 ± 0.8	580400 ± 29000	1.6 ± 0.2	3600 ± 400
12 ± 0.6	5.5 ± 0.6	557400 ± 28000	1.7 ± 0.2	3400 ± 300
25 ± 1.3	11.6 ± 1.2	599000 ± 30000	1.5 ± 0.2	3500 ± 400
38 ± 1.9	10.7 ± 1.1	575700 ± 29000	1.6 ± 0.2	3200 ± 300

Degree of acetylation (DA), weight-average molecular weight (Mw), dispersity (Đ), weight-average degree of polymerization (DPw) defined as the ratio between the weight-average molecular weight of a chitosan chain (Mw) and the molar mass of the constitutive unit of the polymer.

2.2. Preparation, sterilization and storage of chitosan hydrogels

Chitosan physical hydrogels were formed according to a gelation process named aqueous NaOH induced-gelation [41,42]. Purified chitosan (DA=2.5, 12, 24 or 38%) was dissolved in diluted aqueous acetic acid. The amount of acetic acid corresponded to the stoichiometric protonation of the NH_2 sites of chitosan. The resulting chitosan solution (polymer concentrations of 1.5, 1.65, 1.85 or 2.35%, depending on the DA (for DA=2.5, 12, 24 or 38%, respectively)) was centrifuged to remove air bubbles and then poured into a Petri dish with a diameter of 3.5 cm. We obtained chitosan physical hydrogels at a final concentration of approximately 3% (w/w) and with different DAs by putting the polymer solution in contact with concentrated aqueous NaOH (3.0 mol.L-1) for 1 hour. For this, a same volume of NaOH solution was poured over the chitosan solution for the different hydrogels prepared (the amount of chitosan solution was the same for the different hydrogels). Finally, we thoroughly washed the chitosan hydrogels with deionized water until neutral pH and stored them at room temperature in deionized water. Before analysis and implantation into animals, the chitosan physical hydrogels were steam-sterilized under standard conditions (121°C, 1 bar, 20 min). Hereafter, the codification “Ch-X” is used to identify the chitosan hydrogels. The “X” stands for the DA of

chitosan (i.e., Ch-2.5, Ch-12, Ch-24 or Ch-38). The hydrogels were ready to use after the sterilization step.

2.3. Determination of the final polymer concentration in hydrogels

The final chitosan concentration within the hydrogels was determined as described in a previous work [36]. A known weight of chitosan physical hydrogel was freeze-dried, and further, the water content of the freeze-dried hydrogels was precisely determined by thermogravimetric analysis. We can thus deduce the concentration of the polymer within the hydrogel.

2.4. Rheometry analysis

Dynamic-mechanical rheological measurements were carried out by using an ARES rheometer (TA Instruments) operating with a plate-plate geometry (diameter of 25 mm) at room temperature. The strain amplitude was monitored to ensure the measurements were carried out within the linear viscoelastic region, resulting in storage modulus (G') and loss modulus (G'') independent of the strain amplitude. Thus, we carried out angular frequency sweep measurements in the range from 100 rad.s-1 down to 0.1 rad.s-1 (at an applied strain of 0.5%). We repeated these analyses three times for each type of hydrogel ("destructive characterization").

2.5. Suturability tests

The suturability test consisted of making a loose suture in the hydrogel with a suture thread and then gradually increasing the force applied to the thread until the material broke/tore [41]. Gel samples of 10 mm × 10 mm with similar thicknesses (approximately 0.8±0.1 mm) were analyzed using a dynamic mechanical analyzer (DMA Q800, TA 190 Instruments). We punctured each chitosan physical hydrogel at 3 mm of its down edge with a suture thread (Polyvinylidene Fluoride 6/0, PREMIO Peters Surgical). Afterwards, the hydrogel was attached to the upper clamp of the DMA using a tension gripper, and on the other side, the suture thread to the lower clamp. The tensile suture measurements were performed at room temperature in force-controlled mode with a strength ramp of 0.5 $N.min^{-1}$ up to 18.0 N and a preloading strength of 0.01 N, allowing the ultimate suture load to be determined. We repeated such analyses five times for each hydrogel.

2.6. Animals

Fifty-eight male male Wistar rats (Janvier Labs, Genest Saint Isle, France) weighing an average of 200-225 g and twenty female 3 to 5-month-old mice with conditionally invalidation for Serum response factor gene (SRF^{HKO} mice) [44] were used in this study. All procedures were approved by our institutional Ethics Committee "Charles Darwin" (Permit number: #4370) and complied with the European legislation (Directive 2010/ 63/EU) on animal care.

2.7. Cardiac surgery and experimental groups

Myocardial infarction (MI) was induced as described previously [45,46]. Briefly, rats were anaesthetized with isoflurane (Baxter, Maurepas, France), 3% at induction and 2% for maintenance, and tracheally ventilated at a rate of 45 min^{-1} and with a 1 mL average insufflate volume for 100 g of body weight (Harvard Apparatus, France). The heart was exposed through a left thoracotomy and the left coronary artery was permanently ligated between the pulmonary artery trunk and the left atrial appendage. Analgesia was performed for 2 days after surgery with a 10 $mg.kg^{-1}$ intraperitoneal injection of ketoprofen (Merial, Lyon, France).

Four weeks after myocardial infarction, the rats underwent a baseline echocardiographic assessment to evaluate their left ventricular (LV) function. Following a median sternotomy, the animals were then allocated to receive an epicardial implantation of chitosan hydrogels with four different DAs (Ch-2.5, n=9; Ch-12, n=11; Ch-24, n=9; Ch-38, n=13). Four additional rats assigned to a control group (MI) only underwent open-chest placement of similar sutures, without any implantation. One month after treatment, all animals underwent a repeat echocardiographic assessment of LV function and were sacrificed thereafter.

Additional experiments were conducted for the Ch-24 chitosan hydrogel. Briefly, four weeks after myocardial infarction, the rats underwent a median sternotomy to receive an epicardial implantation of Ch-24 chitosan hydrogels or an open-chest placement of similar sutures, without any implantation. The animals were sacrificed one week (n=6 per group) after treatment.

Dilated cardiomyopathy was induced by injection of tamoxifen into conditionally invalidated Serum Response Factor (SRF^{HKO}) mice [44]. Briefly, SRF^{HKO} mice were generated by mating mice harboring a homozygous conditional allele of SRF gene (SRFflox) with a cardiac specific tamoxifen-inducible CreER driver mouse line, which express CreER recombinase under the control of cardiomyocyte specific α-myosin heavy chain promoter. The excision of cardiac SRF gene was induced by daily intraperitoneal tamoxifen injections (20 mg/g/day; Sigma Aldrich, St. Quentin Fallavier, France) on 3 consecutive days. Before tamoxifen administration, the animals were first anaesthetized with isoflurane (Baxter, Maurepas, France) for a baseline echocardiographic assessment and then allocated to receive an epicardial implantation of chitosan hydrogels with two different DAs (Ch-2.5, n=10; Ch-24, n=10). Analgesia was performed for 2 days after surgery with a 10 $mg.kg^{-1}$ subcutaneous injection of ketoprofen (Merial, Lyon, France).

Three weeks after treatment, all animals underwent another echocardiographic assessment of LV function and were sacrificed thereafter. The explanted hearts were separated into two halves by a short-axis section through the midportion of the grafted area. The blocks were immediately fixed in 4% of formaldehyde for 24 h, dehydrated, and embedded in paraffin for histological analysis or

immediately fixed in Tissue-Tek (Sakura Finetek, Villeneuve d'Ascq, France) and frozen in liquid nitrogen-cooled isopentane for immunohistochemical analysis.

2.8. Evaluation of cardiac function

Pre- and post-transplantation cardiac function were evaluated before transplantation and one month thereafter for the myocardial infarction rats and three weeks thereafter for the SRF^{HKO} mice by transthoracic echocardiography of lightly anesthetized animals under isoflurane (induction with 2% and maintained with 0.5%) [8,9]. This noninvasive measurement of left ventricular dimensions and volumes was conducted using echocardiography-Doppler (Vivid 7 Dimension/Vivid7 PRO; GE Medical System Co, Vélizy, France) with an ultrasound probe with a 9 to 14 MHz frequency range. The bidimensionally guided time-motion recording mode (parasternal long-axis view) of the left ventricle (LV) provided the following measurements: diastolic (IVSd) and systolic interventricular septum (IVSs) and posterior wall thicknesses (LVPWd and LVPWs), LV end-diastolic (LVEDD) and end-systolic diameters (LVESD), and heart rate. Each set of measurements was obtained from the same cardiac cycle. The LV shortening fraction (LVSF) was calculated using the formula: (LVEDD-LVESD)/LVEDD×100. LV myocardial volumes, LV end-diastolic (LVEDV), and end-systolic (LVESV) volumes were calculated using a half-ellipsoid model of the LV. From these volumes, LV ejection fraction (LVEF) was calculated using the formula: (LVEDV−LVESV)/LVEDV×100. The LV thickness/LV radius ratio (h/r) was also assessed in all animals. All measurements were performed on digital loops in triplicate and averaged by an investigator blinded to the treatment group.

2.9. Histology and immunolabeling

Ten µm heart sections were made using a microtome (Leica Microsystems, Nanterre, France), stained with hematoxylin and eosin for visualization of general morphology and Sirius red for visualization of fibrosis, mounted in Eukitt resin (CML, France) and examined by transmitted light microscopy. Images were taken with a microscope (Leica Microsystems, Nanterre, France) equipped with a digital camera.

Immunolabeling was performed on ten µm frozen heart sections. The primary antibodies which we used in this study are: anti-caveolin-1α (rabbit IgG, dilution 1:150, Santa Cruz Biotechnologies, Heidelberg, Germany), anti-CD-206 (rat IgG2a, dilution 1:50, Santa Cruz Biotechnology, Heidelberg, Germany) and anti-vinculin (mouse IgG, dilution 1:200, Sigma Aldrich, St. Quentin Fallavier, France). Binding of primary antibodies was detected by incubating the sections with Alexa-conjugated secondary antibodies (dilution 1:1000; Life Technologies). Images were captured using an inverted microscope (Leica Microsystems, DMi8). All images were acquired using identical settings for

exposure for each parameter. All of the measurements were performed blinded to the experimental conditions using ImageJ software (National Institutes of Health [NIH], Bethesda, MD, USA).

The amount of fibrosis was quantified as the Sirius red-positive area/ventricular surface ratio on 6 fields per section on 3 sections per heart, and 5-8 animals per group. Capillary density, defined as the capillary-to-cardiomyocyte ratio, was measured in the same area as the number of caveolin-1-labeled cells (endothelium) over the number of vinculin-positive cells (cardiomyocytes). A minimum of 4 fields per cross-section on 3 cross-sections per heart, and at least 3–5 animals per group were used. The maximal length and width of the cardiomyocytes was measured using ImageJ following vinculin-immunofluorescence staining. At least 500 cardiomyocytes per group were analyzed. Measurements were performed on samples from at least five individuals in each group.

2.10. Relative quantification of gene expression by real-time PCR

Total RNA was extracted from the hearts using TRIzol® (Thermo Fisher Scientific, Saint-Herblain, France) following the manufacturer's instructions. From 500 ng of extracted RNA, the first-strand cDNA was then synthesized using a RevertAid First Strand cDNA Synthesis Kit (Thermo Fisher Scientific, Saint-Herblain, France) with random hexamers according to the manufacturer's instructions. Using the Light Cycler® 480 system (Roche Diagnostics), the reaction was carried out in duplicate for each sample in a 6-µl reaction volume containing 3 µl of SYBR Green Master Mix, 500 nM of the forward and reverse primers each and 3 µl of diluted (1:25) cDNA. The thermal profile for the SYBR Green qPCR was 95°C for 8 min, followed by 40 cycles at 95°C for 15 s, 60°C for 15 s and 72°C for 30 s. To exclude PCR products amplified from genomic DNA, primers were designed, when possible, to span one exon-exon junction. The mean gene expression stability of 2 genes, Hmbs (hydroxymethylbilane synthase) and B2M (beta-2-microgobulin), were used as the reference transcripts. Data were collected and analyzed using the LightCycler® 480 software release 1.5.0 (Roche Diagnostics).

2.11. Cytokine quantification by antibody array

The protein concentration was measured using a bicinchoninic acid kit (Sigma Aldrich, St. Quentin Fallavier, France) with bovine serum albumin as a standard. Cytokine antibody arrays were carried out according to the manufacturer's instructions (Abcam, USA) using 200 µg of protein per sample. Expression of 38 different cytokines was quantified by measuring the intensity of the different spots using ImageJ software (National Institutes of Health [NIH], Bethesda, MD, USA).

2.12. Peptide and protein analysis by liquid chromatography tandem-mass spectrometry (LC-MS/MS)

Total proteins were extracted from the heart samples by homogenization in 400 µL of ice-cold lysis buffer containing: 50 mM Tris (pH 8), 0.1% SDS, 50 mM NaCl, 1 mM EDTA, 1% Triton, and 1 mM

DTT with protease and phosphatase inhibitor cocktails (Sigma Aldrich, St. Quentin Fallavier, France). The supernatant was collected after centrifugation at 12 000 *g* for 5 min at 4 °C. The protein concentration was measured using a bicinchoninic acid kit (Sigma Aldrich, St. Quentin Fallavier, France) with bovine serum albumin as a standard. For LC-MS/MS acquisition, 50 µg of protein for each sample was precipitated with cold acetone overnight at –20 °C. Proteins were digested overnight at 37°C in 20 µL of 25 mM NH_4HCO_3 with 1.25 µl sequencing grade trypsin (0.2 µg/µL, Promega Corporation, WI, USA). Peptide mixtures were desalted and concentrated on ZipTip µ-C18 pipette tips (Millipore). Peptides were separated by chromatography with the following parameters: Acclaim PepMap100 C18 precolumn (2 cm, 75 µm i.d., 3 µm, 100 Å), Pepmap-RSLC Proxeon C18 column (50 cm, 75 µm i.d., 2 µm, 100 Å), 300 nL/min flow rate, a 98 min gradient from 95% solvent A (water, 0.1% formic acid) to 35% solvent B (100% acetonitrile, 0.1% formic acid) followed by column regeneration, giving a total time of 120 minutes. Peptides were analyzed in the Orbitrap cell at a resolution of 70,000, with a mass range of m/z 375–1500. MS/MS data were acquired in the Orbitrap cell in a Top20 mode, with an AGC target of 3.106 for full MS. Fragments were obtained by Higher-energy C-trap Dissociation (HCD) activation with a collisional energy of 27% and a quadrupole isolation window of 1.4 Da, with an AGC target of 2.105. MS/MS data were acquired by an Orbitrap in a data-dependent mode with a dynamic exclusion of 30 seconds. Peptides with unassigned charge states or monocharged were excluded from the MS/MS acquisition. The maximum ion accumulation times were set to 50 ms for MS acquisition and 45 ms for MS/MS acquisition.

For the peptide and protein identification step, all MS and MS/MS data were processed with Proteome Discoverer software (Thermo Scientific, version 2.2) and with the Mascot search engine (Matrix Science, version 5.1). The mass tolerance was set to 7 ppm for precursor ions and 0.5 Da for fragments. The following variable modifications (maximum two per peptide) were allowed: oxidation (M), phosphorylation (ST), and acetylation (*N*-term of protein). The maximum number of missed cleavages was limited to two for the trypsin protease. The SwissProt database (02/17) with the *Rattus norvegicus* taxonomy was used for the MS/MS identification step. Peptide identifications were validated using a 1% FDR (false discovery rate) threshold calculated with the Percolator algorithm.

Label Free quantitation was performed using Progenesis QI for proteomics software (Waters). Data were processed with Proteome Discoverer 2.4 software (Thermo Fisher Scientific) using the HI-3 method for quantification of proteins. Identification was performed on a Mascot search server (Matrix Science; version 2.4) used in Proteome Discoverer 2.4. The mass tolerance of the fragment ions was set to 6 ppm for precursor ions and 0.02 Da for fragments. Identification of tryptic peptides related to the proteins were performed using the *Mus musculus or Rattus Norvegicus* database from Uniprot RefSeq. Post translation modifications were searched in the dynamics parameters: oxidation (M), phosphorylation (S/T/Y), and acetylation (K/N-terminal). The maximum number of missed cleavages was limited to two for trypsin digestion. P-values of the peptides were calculated using the percolator

algorithm, and a 1% filter was applied as a false-discovery rate threshold. Abundance variations of proteins with a p-value under 0.1 obtained from ANOVA and a maximum fold change of 1.5 were further considered.

2.13. Statistical Analysis

Analyses were conducted using GraphPad Prism 7.00 (GraphPad Software Inc., SD, USA). For one-way analysis of variance, the normality was checked using the Shapiro-Wilk normality test. If the normality of distribution assumption was not met, the nonparametric Mann-Whitney test was used instead of ANOVA. If a significant difference was found, then multiple comparison tests were performed to compare the different groups analyzed (Dunn's or Dunnett's multiple comparison test following a nonparametric or parametric test, respectively). For statistical analysis of cardiomyocyte size distribution, Kolmogorov-Smirnov tests were used. Grouped data were analyzed using two-way ANOVA, followed by post hoc Holm-Sidak tests for multiple comparisons when an interaction between the main factors reached significance. A p-value < 0.05 was considered significant. Values are given as the means ± standard error of the mean (SEM).

3. Results

In this study, we investigated the impact of chitosan hydrogel patches with different DAs on cardiac tissue regeneration using two murine models of cardiomyopathy. First, we described the formation of hydrogel patches composed of only water and pure chitosan with different DAs and then we characterized their mechanical properties before epicardial implantation in animals.

3.1. Preparation of chitosan hydrogels with different degrees of acetylation

We investigated the impact of DA on the mechanical and biological properties of hydrogels in order to define an optimal DA for the design of a cardiac patch. It should be noted that we have chosen a wide chitosan DA range, starting from a DA of 2.5% (i.e. the DA of initial deacetylated Mahtani chitosan) up to a maximum DA to obtain stable gels (38%). Indeed, above 40%, chitosans re-acetylated in the solution state remain soluble over a wider pH range and it is not possible to obtain stable gels by neutralization of a chitosan aqueous solution either with ammonia vapors or sodium hydroxide solutions. We first produced gels with different DAs (2.5%, 12%, 24% and 38%) while having the same final polymer concentration (~ 3% (w/w)). To prepare these hydrogels with different DAs, we needed to N-reacetylate the chitosan that we purchased (initial DA of 2.5%). As described previously [34,35], the conditions of acetylation were sufficiently mild to avoid any chain degradation. As described in Table 1, these acetylations allowed for the production of a homogeneous series of chitosans of different DAs with similar degrees of polymerization.

Macroscopically, shrinkage was observed for all hydrogels after the gelation step (a slight decrease in diameters in the Petri dishes). This phenomenon was previously reported [41] for the same kind of chitosan hydrogels at low DA, and for another kind of physical chitosan hydrogel [36]. Meanwhile, the shrinkage led to significant changes in polymer concentration. Thus, the final polymer concentrations were measured for various sterilized hydrogels of different DAs and are reported in **Figure 1.** The experimental data demonstrated a linear correlation between the initial polymer concentration in the chitosan solution and the concentration of polymer in the final hydrogels regardless of the DA. The increase in concentration was more important at a lower DA and at a lower polymer concentration. A higher polymer concentration induces a more entangled system less likely to shrink during gelation. Accordingly, from these data, we can deduce the least square fit relationship between the polymer concentration in the solution and in the gel (% (w/w)):

$$[\text{Chitosan}]_{\text{Gel}} = (-0.0106\ \text{DA} + 1{,}2731)\ [\text{Chitosan}]_{\text{Sol}} + 0.0095\ \text{DA} + 0.636 \quad / \text{eq (1)}$$

Such a relationship is probably impacted by the molar mass distribution of the polymer.

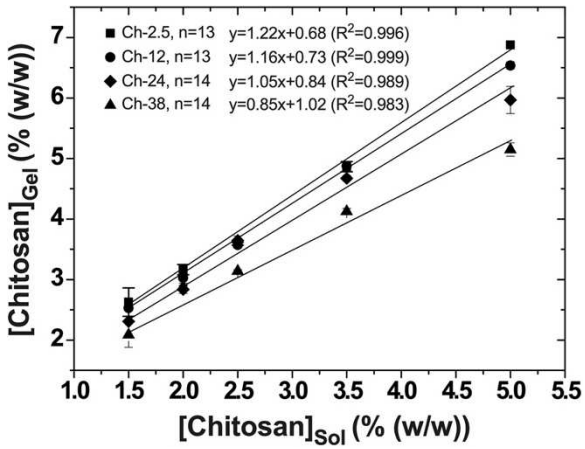

Figure 1. Final hydrogel concentration ([Chitosan]$_{Gel}$) after neutralization with a NaOH solution (3 M, 1 h) and autoclave sterilization, with different degrees of acetylation (Ch-2.5, Ch-12, Ch-24 and Ch-38 hydrogels) with different polymer solution concentrations ([Chitosan]$_{Sol}$).

Chitosan dissolves in acidic aqueous solution via the protonation of its NH_2 sites. In the solution state, before the gelation process, chitosan behaves as a highly entangled polyelectrolyte (polycation bearing $-NH_3^+$ groups), and apparently its charge density decreases with the DA. For high DA values, the polysaccharide can be considered as a polymer bearing isolated charges, with a hydrophobicity increasing with the DA [36,47].

The gelation process conceptually consists of the modification of the balance between hydrophilic and hydrophobic interactions within the system, favoring interchain hydrophobic interactions: this change could be achieved here thanks to a decrease in the apparent charge density of chitosan induced by neutralization. Then, interchain interactions occur and result in the formation of a network combining hydrophobic interactions, H-bonding and high functionality physical crosslinks constituted by crystallites [42].

The observed shrinkage phenomenon is less important for chitosan gels with a high DA than chitosan gels with a low DA. At a low DA, chitosan chains present a maximal hydrophilic contrast between the protonated and neutralized forms. Thus, after the gelation process, high DA chitosan is more hydrophilic than low DA chitosan due to the presence of many polar acetyl groups present in the polymer chains. This residual hydrophilicity, together with a lower impact of protonation on the conformation, could explain why chitosan hydrogels with high DA exhibit less shrinkage.

Moreover, it is worth noting that the sterilization process also induced a slight increase in the polymer concentration. This increase was higher at low DA (see the examples in **Table 2**). These results are in accordance with previous results reported for sterilized chitosan physical hydrogels [36,41]. During the sterilization step, the temperature increases up to 121°C lead to a decrease in hydrogen bonds in favor of hydrophobic interactions [41], resulting in shrinkage. Again, such effects are limited at high DAs, since the chitosan keeps its residual hydrophilicity.

Table 2. Concentration of polymers in chitosan gels before and after sterilization.

Degree of acetylation (%)	Concentration of the initial solution (%) (w/w)	Concentration of the corresponding final gel before sterilization (%) (w/w)	Concentration of the corresponding final gel after sterilization (%) (w/w)	Percentage of concentration increase induced by the sterilization (%)
2.5%	5	5.83 ± 0.05	6.88 ± 0.93	18
12%	5	5.66 ± 0.44	6.54 ± 0.06	15
24%	5	5.55 ± 0.26	5.97 ± 0.22	8
38%	5	5.15 ± 0.09	5.28 ± 0.11	3

Thus, in this study dealing with the effect of DA on gel properties, each hydrogel was prepared in order to have a final concentration within the hydrogels of approximately 3% (w/w) after sterilization, regardless of the DA. As the shrinkage was different depending on the DA, the concentration of chitosan in the initial solution had to be adapted for each DA (see eq. 1) in order to obtain the same final concentration of approximately 3% (w/w).

Hydrogels formed with chitosans of high DAs seemed to be more flexible than hydrogels formed with chitosans of low DAs (**Figure 2C**). Macroscopically, the hydrogels prepared from chitosan DA=38% were softer, more flexible and translucent. In contrast, the use of chitosan DA=2.5% resulted in harder hydrogels that were easy to manipulate and more opaque. This change in opacity might come from the differences of the microstructure of the hydrogels. All hydrogels are composed of interpenetrated submicrometric gel aggregates constituting the material structure [48,49]. These aggregates may present different diffusion properties depending on the DA of chitosan. The mechanical properties of these hydrogels were then evaluated by carrying out rheological measurements, tensile tests, and suturability tests.

3.2. Higher DA results in chitosan hydrogels with lower viscoelastic moduli and suturability

The rheological study allowed us to compare the viscoelasticity of the different hydrogel patches developed in this work. We carried out rheological measurements to study the evolution of storage and loss moduli as a function of DA. For all hydrogels, the moduli were nearly frequency-independent and G' was at least ten times higher than G'' (see an example of the curves of the storage and loss moduli in **Figure 2A)**, in accordance with the definition of a gel [50]. Consistent with physical gels [51,52], a very slight decrease in the G' and a very slight increase in G" at low frequencies are observed for our gels (**Figure 2A**). The equilibrium storage modulus, noted here as Ge', was estimated corresponding to the value of G' at the plateau for low frequencies. The value of Ge' for the different hydrogels (DA: 2.5, 12, 24, and 38%) was reported in Figure 2B (**Figure 2B)**. As already mentioned, all of the hydrogels were steam-sterilized before mechanical characterizations. In this concentration range,

previous works reported that this sterilizing treatment has a low impact on the mechanical properties of chitosan hydrogels through the viscoelastic moduli and ultimate suture strength [41].

In the DAs range investigated, we observed a decrease in Ge' with increasing DAs. These results are in line with the semiquantitative experiments shown in **Figure 2C** and with the literature [37,42]. The presence of N-acetyl glucosamine residues in chitosan chains contributes to a reduction in the charge density of the polyelectrolyte chains. As a consequence, this leads to the limitation of chain extension in solution and the decrease of entrapped macromolecular entanglements (i.e. "interchain cross-links") in the gel. In addition, Montembault *et al.* showed that the viscosity of chitosan solutions decreased with increased DA [36].

Conversely, at a low DA, the chain extension due to strong electrostatic repulsions (polyelectrolyte behavior), as a result of the elevated charge density of the chains, induced a high level of entanglement of the chitosan macromolecules. The gelation of more entangled systems leads to hydrogels with higher mechanical properties. In this work, the gelation was fast enough to preserve entanglements in the gel (gelation by neutralization in a NaOH bath at 3.0 mol.L^{-1}), resulting in mechanically improved hydrogels at lower DAs.

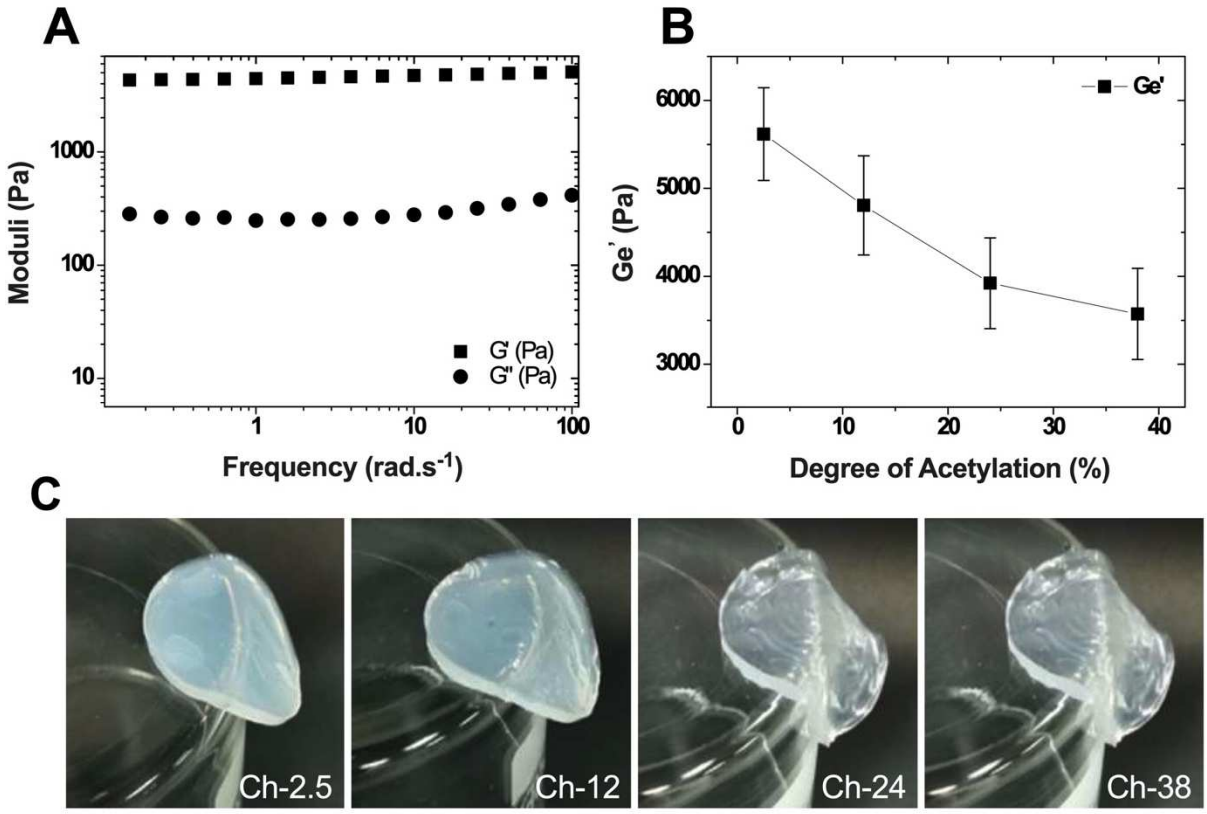

Figure 2. Mechanical characterization of chitosan hydrogels. (A) Evolution of the storage and loss moduli for a Ch-12 hydrogel. (B) Influence of the DA on the equilibrium elastic modulus (Ge') of the chitosan hydrogels. (C) Hydrogels obtained from chitosans of different degrees of acetylation (2.5, 12, 24, and 38%) and with the same final polymer concentration ($[Chitosan]_{Gel}$~3% (w/w)).

In the context of our application, the design of hydrogel implants requires evaluation of their suture properties. Thus, different hydrogel membranes were prepared to investigate and compare their suture resistance in a quantitative way. The test consists of making a loose suture in the hydrogel and progressively increasing the load applied to the suture until the extraction of the suture (**Figure 3A**). This ultimate suture strength can be defined as "suturability".

As we demonstrated in previous works that the suturability increased with the gel thickness [41], we normalized the different measured suturability values with respect to sample thickness. Our results demonstrated that the normalized suturability decreased with increasing DA, consistent with the rheological measurements: for the Ch-2.5 hydrogel, the value was 0.35 ± 0.04 $N.mm^{-1}$ while for the Ch-38 hydrogel value it was 0.03 ± 0.01 $N.mm^{-1}$ (**Figure 3B**).

Moreover, regardless of the degree of acetylation, *in vivo* preliminary tests indicated that no tears were observed after fixation by suture points. These tests allowed us to ensure that these patches were compatible with surgical practice.

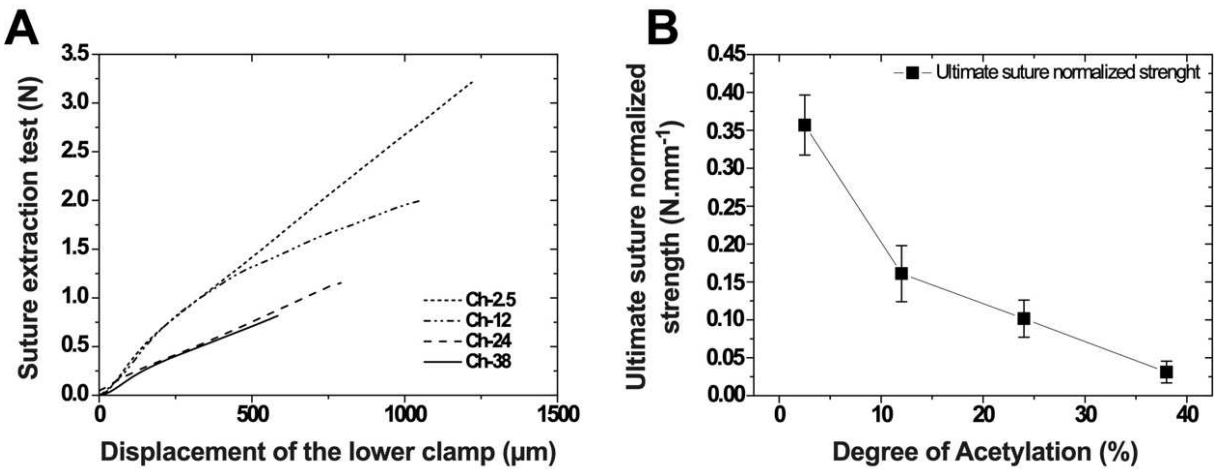

Figure 3. Suturability characterization of the chitosan hydrogels. (A) Normalized static strength diagram of chitosan hydrogels as a function of the DA of chitosan. (B) Ultimate suture normalized strength diagram of chitosan hydrogels as a function of the DA of chitosan.

3.3. Chitosan hydrogels with the highest DAs improved cardiac function after epicardial implantation in myocardial infarction

The potential benefit of epicardial implantation of chitosan hydrogels at different DAs was first evaluated in a rat model of myocardial infarction. One month after the implantation, the chitosan hydrogels were macroscopically visualized on the surface of the hearts (**Figure 4**). We noticed a visible degradation at higher DAs (Ch-24 and Ch-38 hydrogels). For a closer analysis, serial heart sections were made and some of these sections were stained with hematoxylin and eosin to analyze the general aspect of the hydrogels, as well as foreign body responses with respect to inflammation, granulomatous reactions and epicardial fibrosis (**Figure 4A**). All implanted hydrogels were visible on

the surface of the hearts with hematoxylin and eosin staining at one month after implantation. Low DA hydrogels (Ch-2.5 and Ch-12 hydrogels) showed partial degradation accompanied by mononuclear cell infiltration. In contrast, at high DAs (Ch-24 and Ch-38 hydrogels), the chitosan hydrogels were highly degraded after implantation and only small fragments of hydrogels were visible at one month in the grafted area. No exuberant fibrosis and no multinucleated giant cells were visible in the grafted area, demonstrating the absence of a foreign body reaction and the perfect biocompatibility of these chitosan hydrogels at all of the DAs.

In parallel to morphological assessment, we also evaluated the functional impact of epicardial implantation of the Ch-2.5, Ch-12, Ch-24 and Ch-38 hydrogels using transthoracic echocardiography before (baseline) and one month after implantation (**Figure 4B**). We first measured two surrogate heart function parameters, left ventricular ejection fraction (LVEF) and left ventricular shortening fraction (LVSF). Neither LVEF nor LVSF differed at baseline between the groups, thereby suggesting initial ischemic injuries of similar extents. However, after implantation of the chitosan hydrogels, the changes were markedly different between the DAs. As demonstrated in Figure 4B, both LVEF and LVSF significantly increased one month after implantation in the presence of the patch in comparison to MI, except for the Ch-2.5 group. For Ch-2.5, the LVEF and LVSF values tended to remain stable in comparison to MI.

This effect was primarily the result of a decrease in LVESV from baseline values in Ch-24 and Ch-38 hydrogels treated hearts whereas in MI these parameters were increased (**Figure 4B)**. Hearts treated with low DA hydrogels featured a smaller increase in LVESV from baseline values compared with MI. In contrast, the LVEDVs did not differ among the groups (**Figure 4B)**. Echocardiographic data were recorded at similar heart rates.

The improvement of systolic function in transplanted rats was further supported by histological analysis. We quantified the capillary density and the extent of interstitial fibrosis in the border zone of the infarcted area. Our results demonstrated no difference in the mean number of capillaries per cardiomyocytes in the border zone between the different treatment groups (**Figure 4C**). The extent of fibrosis was assessed by Sirius red staining. As demonstrated in **Figure 4D**, the mean percentage area of fibrosis was significantly lower for the Ch-24 hydrogel compared to MI. The extent of fibrosis was also lower with the Ch-12 hydrogel but the differences failed to reach a significant level. Taken together, our results demonstrated that the optimal hydrogel for cardiac applications was the Ch-24 hydrogel.

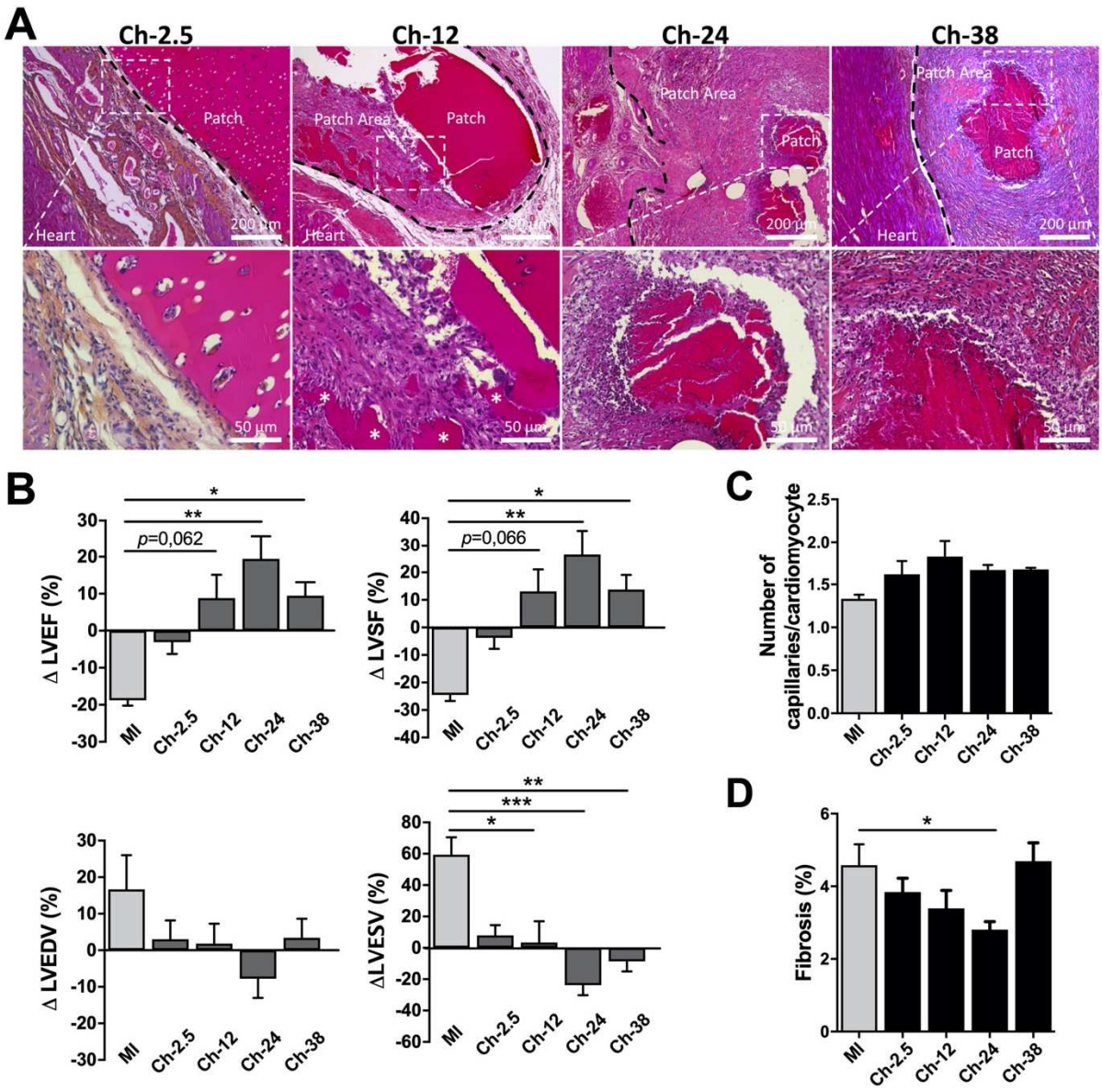

Figure 4. Evaluation of chitosan hydrogels after one month post epicardial implantation in the infarcted hearts. (A) Hematoxylin and eosin staining of the rat heart implanted with different DA of chitosan (2.5%, 12%, 24%, 38%). White asterisks (*) in bottom Ch-12 panel shows remaining chitosan hydrogel fragments; Black dotted lines represent the border between the implanted hydrogels (red) and the heart; White dotted lines (upper panel) show a higher magnification area (of the lower panel). (B) Functional evaluation of chitosan hydrogels after one month post epicardial implantation (n=9–14 per group). (C) Capillary density per cardiomyocyte was evaluated in the left ventricle by caveolin-1α (endothelial cells) and vinculin (cardiomyocyte) immunostaining (n=3–5 per groups). (D) Assessment of cardiac fibrosis by Sirius red staining in the border zone (n=6–10 per group). Note that fibrosis was expressed as the ratio (%) of the area of fibrosis to the whole area of the left ventricle. MI, myocardial infarction. Values are given as the means ± standard error of the mean. *p<0.05; **p<0.01; ***p<0.001.

To elucidate the molecular mechanisms implicated in the improvement of systolic function and decreased extent of fibrosis in the animals treated with Ch-24 hydrogel compared to MI, we examined the mRNA expression of pro-hypertrophic stress, fibrosis, and pro-inflammatory cytokines markers by quantitative real-time PCR (**Figure 5**). Analyses were performed 7 days after epicardial implantation

of the Ch-24 hydrogel to detect changes occurring during the early phase of cardiac remodeling. As demonstrated in **Figure 5A,** mRNA expression of all investigated molecules involved in pro-hypertrophic stress and the development of fibrosis were decreased after Ch-24 hydrogel treatment compared to MI. However, mRNA expression of all investigated pro-inflammatory cytokines markers was similar between treated and nontreated animals (**Figure 5B**).

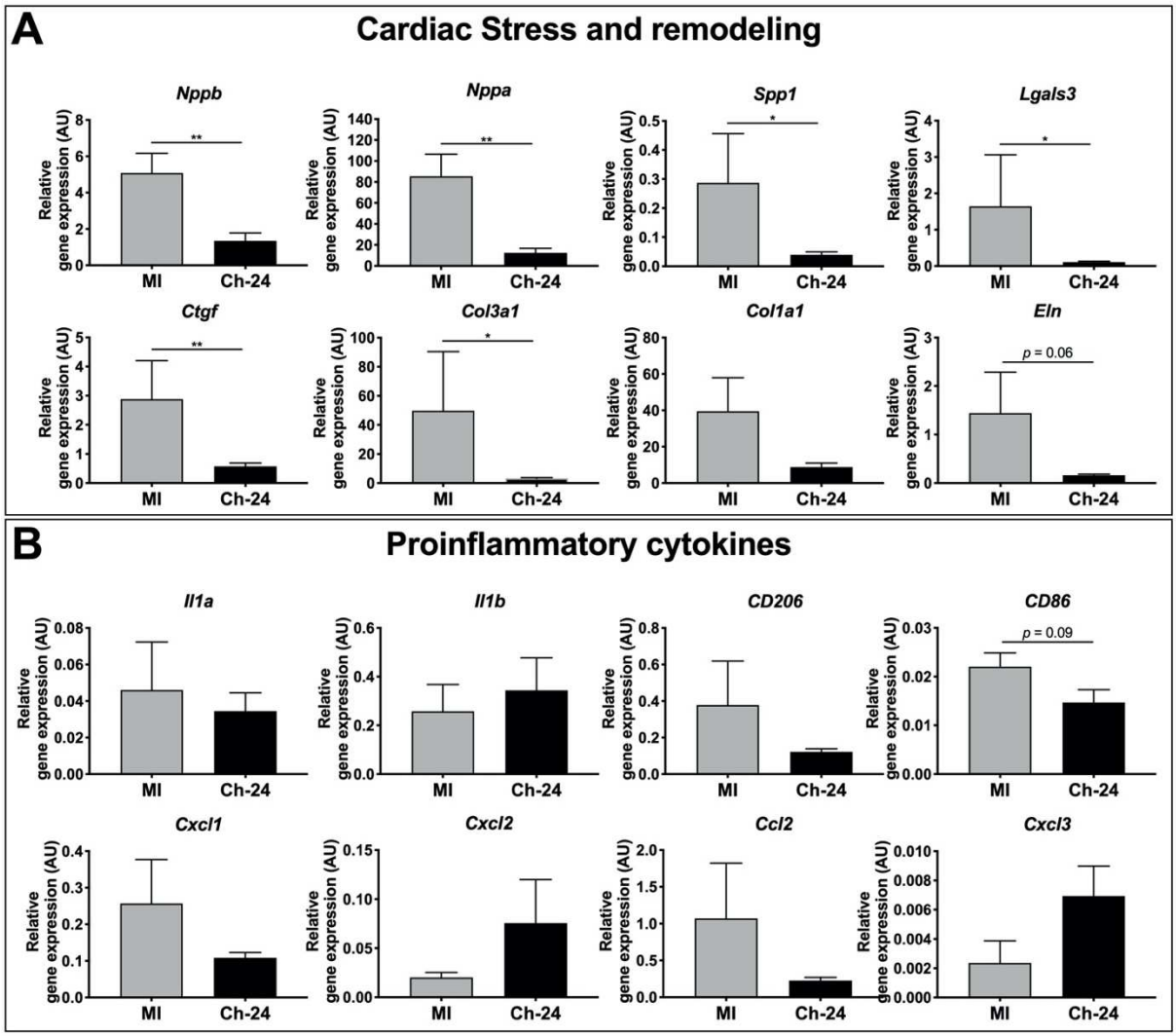

Figure 5. Evaluation of chitosan hydrogels after 7 days post epicardial implantation in the infarcted hearts. Relative gene expression of selected cardiac stress and remodeling markers (A) and proinflammatory cytokines markers (B) were evaluated after 7 days of implantation in a rat model of chronic myocardial infarction (n=6 per group). MI, myocardial infarction. Values are given as the means ± standard error of the mean. *p<0.05; **p<0.01.

Following these results demonstrating the absence of differences of mRNA expression profiles of pro-inflammatory markers, we investigated the inflammatory response at the protein level. The immunostaining for CD206, a marker of activated macrophages [53], showed no differences between treated and nontreated animals at both 7 and 30 days after epicardial implantation (**Figure S1**). Finally, the degree of inflammatory response after treatment with the Ch-24 hydrogel compared to MI was investigated by cytokine array 7 days after implantation. Cytokine arrays are an antibody-pair-

based assay that allows for the screening of multiple mediators, including activin A, agrin, CD86, cytokine-induced neutrophil chemoattractants (CINC), ciliary neurotrophic factor (CNTF), Fas ligand, fractalkine, granulocyte macrophage-colony stimulating factor (GMSF), intercellular adhesion molecule 1 (ICAM-1), interferon-γ (IFN-γ), interleukins, leptin, LPS-induced CXC chemokine (LIX), L-selectin, monocyte chemotactic protein 1 (MCP-1), macrophage inflammatory protein 3α (MIP-3α), metalloproteinase 8 (MMP-8), neural growth factor β (NGF-β), platelet-derived growth factor AA (PDGF-AA), prolactin R, RAGE, chemokine-1, tissue inhibitor of metalloproteinase 1 (TIMP-1), tumor necrosis factor α (TNFα) and vascular endothelial growth factor (VEGF). As shown in Table 3, no differences were observed after 7 days of epicardial implantation of the Ch-24 hydrogel compared to MI, demonstrating that the positive impact of chitosan on cardiac remodeling and function is probably independent of its role as a modulator of the inflammatory response.

Table 3. Cytokine antibody array data from the animals received Ch-24 chitosan hydrogel. Cytokine antibody arrays were carried out 7 days after epicardial implantation of chitosan hydrogels in infarcted myocardium. The system allows us to screen multiple mediators. The intensities of the different spots were determined by using densitometric software (n=5 mice per group). MI, myocardial infarction. Values are given as the means ± standard error of the mean.

Cytokine	MI	Ch-24
Activin A	154 ± 12	169 ± 39
Agrin	2791 ± 447	3293 ± 432
CD86	100 ± 19	98 ± 23
CINC-1	441 ± 32	537 ± 106
CINC-2a	200 ± 9	292 ± 43
CINC-3	250 ± 25	365 ± 76
CNTF	190 ± 44	133 ± 21
Fas Ligand	49 ± 14	47 ± 17
Fractalkine	54 ± 17	80 ± 21
GM-CSF	232 ± 22	261 ± 50
ICAM-1	258 ± 48	197 ± 59
IFN-g	88 ± 24	82 ± 32
IL-1a	389 ± 72	540 ± 72
IL-1b	105 ± 35	122 ± 29
IL-1 R6	321 ± 48	279 ± 48
IL-2	60 ± 16	55 ± 16
IL-4	107 ± 25	70 ± 22
IL-6	74 ± 11	101 ± 22
IL-10	123 ± 34	99 ± 28
IL-13	99 ± 49	103 ± 42
Leptin	59 ± 23	50 ± 12
LIX	233 ± 50	275 ± 52
L-Selectin	149 ± 29	127 ± 29
MCP-1	174 ± 56	190 ± 65
MIP-3a	185 ± 36	218 ± 17
MMP-8	259 ± 152	195 ± 58
NGFb	184 ± 36	208 ± 27
PDGF-AA	220 ± 28	265 ± 14
Prolactin R	173 ± 37	177 ± 16

RAGE	69 ± 7	84 ± 13
Thymus Chemokine-1	1619 ± 458	1391 ± 414
TIMP-1	323 ± 88	249 ± 62
TNFa	128 ± 22	99 ± 30
VEGF	283 ± 59	253 ± 53

Additionally, we analyzed the global protein expression in response to chitosan hydrogel implantation using label-free proteomic analysis to better understand the signaling pathways underlying the benefits of chitosan on cardiac function. Protein extracts from the left ventricle were submitted to mass spectrometry analysis and all identified proteins (n=2598) are presented in **Figure 6**. Significantly down- (max fold change ≤ -1.5 and p-value ≤ 0.1) and upregulated (max fold change ≥ 1.5 and p-value ≤ 0.1) proteins were computed using the KEGG database for identification of protein functions and their involvement in signaling pathways. Significantly modified proteins are presented in **Supplementary Table 1**. Mitochondrial proteins, NADH dehydrogenase subunit 5 (accession number P11661), translocase of outer mitochondrial membrane 34 (Q3KRD5), isocitrate dehydrogenase (Q5XIJ3) involved in the tricarboxylic acid cycle, and short-chain specific acyl-CoA dehydrogenase (P15651) involved in fatty acid degradation were downregulated with Ch-24 compared to MI. On the other hand, cytosolic proteins involved in the glycolysis process, such as alcohol dehydrogenase (P06757) and phosphoglycerate mutase 1 (P25113), were upregulated with the Ch-24 hydrogel. Proteins involved in immune responses, such as fibrinogen beta chain (P14480), complement C5 (A0A1B0GWS5) and serum amyloid P-component (P23680) were also found to be upregulated with the Ch-24 hydrogel compared to MI.–Finally, a higher expression of pre-mRNA processing factor spliceosome protein (B5DFM8) and cytoskeletal proteins troponin I (P23693) and desmin (Q6P725) were found after chitosan patch treatment.

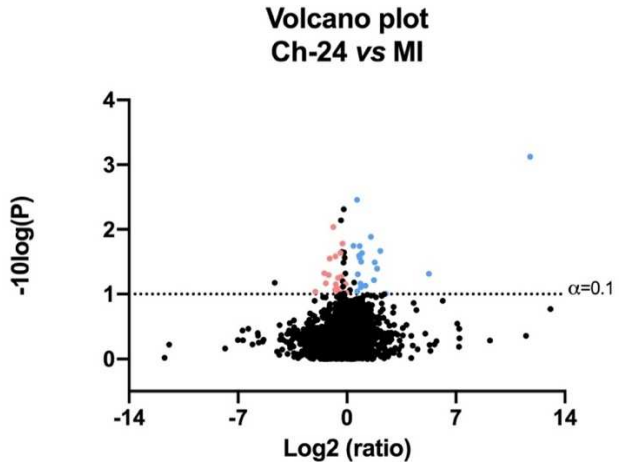

Figure 6. Volcano plot representation of quantitative label-free proteomics analysis of Ch-24 hydrogel treated heart compared to MI. All proteins identified are displayed according to their fold change relative to MI (x-axis: log2) as well as its statistical significance (y-axis: –log10 (p-value)). Proteins highlighted in red are negatively regulated (max fold change ≤ -1.5 and p-value ≤ 0.1), and proteins highlighted in blue are positively regulated (max fold change ≥ 1.5 and p-value ≤ 0.1) compared to MI.

3.4. Chitosan hydrogels with DA 24% improve cardiac function and prevent cardiac remodeling in a mouse model of dilated cardiomyopathy

To broaden the spectrum of possible application of this promising therapeutic approach, we also implanted chitosan hydrogels in a nonischemic dilated cardiomyopathy model, the SRF^{HKO} mouse model. Twenty SRF^{HKO} mice received the Ch-2.5 (n=10) and Ch-24 (n=10) hydrogels after tamoxifen injection, before the onset of the dilated cardiomyopathy, to evaluate the impact of chitosan hydrogels on adaptive cardiac remodeling. First, we evaluated the functional impact of epicardial implantation of the Ch-2.5 and Ch-24 hydrogels using transthoracic echocardiography before (baseline, one week after tamoxifen injection) and three weeks after implantation (sacrifice, 4 weeks after tamoxifen injection) (**Figure 7**). At baseline, the LVSF did not differ among the groups. Three weeks after implantation, the LVSF was significantly decreased from the baseline in both the Ch-2.5 and Ch-24 hydrogel groups, but this decrease was lower in Ch-24 compared to the Ch-2.5 hydrogels (**Figure 7A**). This effect was primarily the result of a lower increase in LVESD from baseline values in the Ch-24 compared to the Ch-2.5 hydrogels (**Figure 7B**). LVEDD was increased in both the Ch-2.5 and Ch-24 hydrogels (**Figure 7C**).

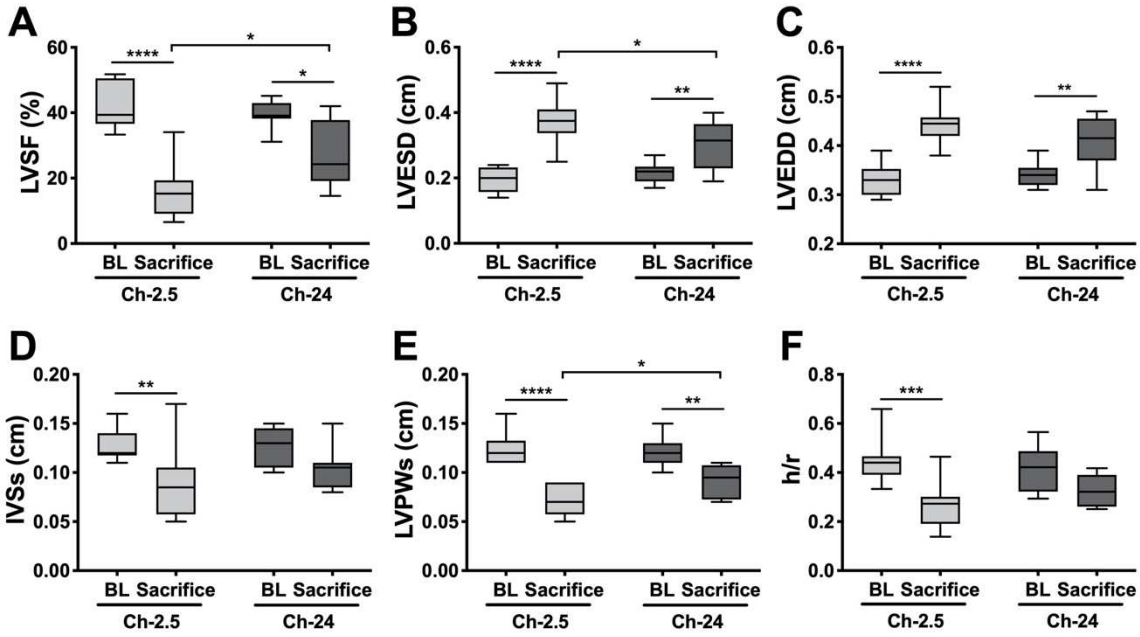

Figure 7. Evaluation of epicardial-implanted chitosan hydrogels in a mouse model of dilated cardiomyopathy. Impact on cardiac function of the epicardial implantation of Ch-24 versus Ch-2.5 hydrogels was evaluated before (BL, baseline) and three weeks after implantation (Sacrifice) in a mouse model of dilated cardiomyopathy based on cardiac-specific and tamoxifen-inducible invalidation of serum response factor. (A) Left ventricular shortening fraction (LVSF); (B) Left ventricular end-systolic diameter; (C) Left ventricular end-diastolic diameter; (D) Interventricular septum thickness in systole (IVSs); (E) Left ventricular posterior wall thickness in systole (LVPWs); (F) Left ventricular thickness to left ventricular radius ratio (h/r). Data are represented in the box plot. The boxes represent the lower to upper quartile range, the error bars represent the entire range, the horizontal bar represents the median value and the dot points represent mean values. *p<0.05; **p<0.01; ***p<0.001; ****p<0.0001.

For a closer analysis of systolic function, we also evaluated systolic interventricular septum (IVSs) and posterior wall thickness (LVPWs) in the treated animals. The IVSs thickness was maintained over the three week period in Ch-24 treated SRF^{HKO} mice but was thinner in Ch-2.5 treated SRF^{HKO} mice at the time of sacrifice (**Figure 7D**). Both the Ch-2.5 and Ch-24 groups exhibited a significant decrease in LVPWs at the time of sacrifice compared to baseline (**Figure 7E**), but the thinning was significantly less pronounced in Ch-24 treated mice compared to Ch-2.5 treated mice at the time of sacrifice. Finally, we calculated the LV thickness to LV radius ratio (h/r), which has a constant relationship with left ventricular systolic wall stress [54]. We demonstrated that the LV h/r ratio was significantly decreased in Ch-2.5 compared to Ch-24 treated animals, indicating that Ch-24 limits the process of LV chamber dilatation (**Figure 7F**). The functional efficiency of Ch-24 compared to Ch-2.5 during the establishment of heart failure was reinforced by the demonstration of a reduction in the expression of the stress-induced *Nppa* ($p<0.05$), *Nppb* ($p<0.05$) and *Myh7* ($p=0.067$) in Ch-24 treated SRF^{HKO} mice compared to the Ch-2.5 treated ones (**Figure 8A-C**).

To evaluate the impact of the chitosan hydrogels on cardiac remodeling, we also analyzed cardiomyocyte size (**Figure 8D-G**) and cardiac fibrosis (**Figure 8H-J**) in Ch-2.5 and Ch-24 hydrogels treated SRF^{HKO} mice. Fibrosis was measured by Sirius red staining (**Figure 8H**). At the time of sacrifice, all of the SRF^{HKO} mice exhibited interstitial fibrosis (**Figure 8H**). Nevertheless, the mean percentage area of fibrosis was lower in the Ch-24 hydrogel treated mice compared to the Ch-2.5 hydrogel treated group (**Figure 8I**). The reduction in fibrosis was also supported by real-time PCR, which demonstrated significantly less induction of the expression of *Ctgf* in Ch-24 hydrogel treated animals in comparison to Ch-2.5 hydrogel treated ones (**Figure 8J**).

Finally, we conducted morphometrical analysis after vinculin immunostaining to measure the maximal length and width of the cardiomyocytes three weeks after treatment. In SRF^{HKO} mice treated with Ch-2.5 compared to Ch-24 hydrogels, the cardiomyocyte length distribution was shifted toward the higher values whereas the cardiomyocyte width distribution was shifted toward the lower values (**Figure 8D-E**). Moreover, the cardiomyocyte length to width ratio was significantly lower in Ch-24 hydrogel compared to Ch-2.5 hydrogel treated mice, indicating that Ch-24 hydrogel treatment prevents cardiac remodeling in a mouse model of dilated cardiomyopathy (**Figure 8F**).

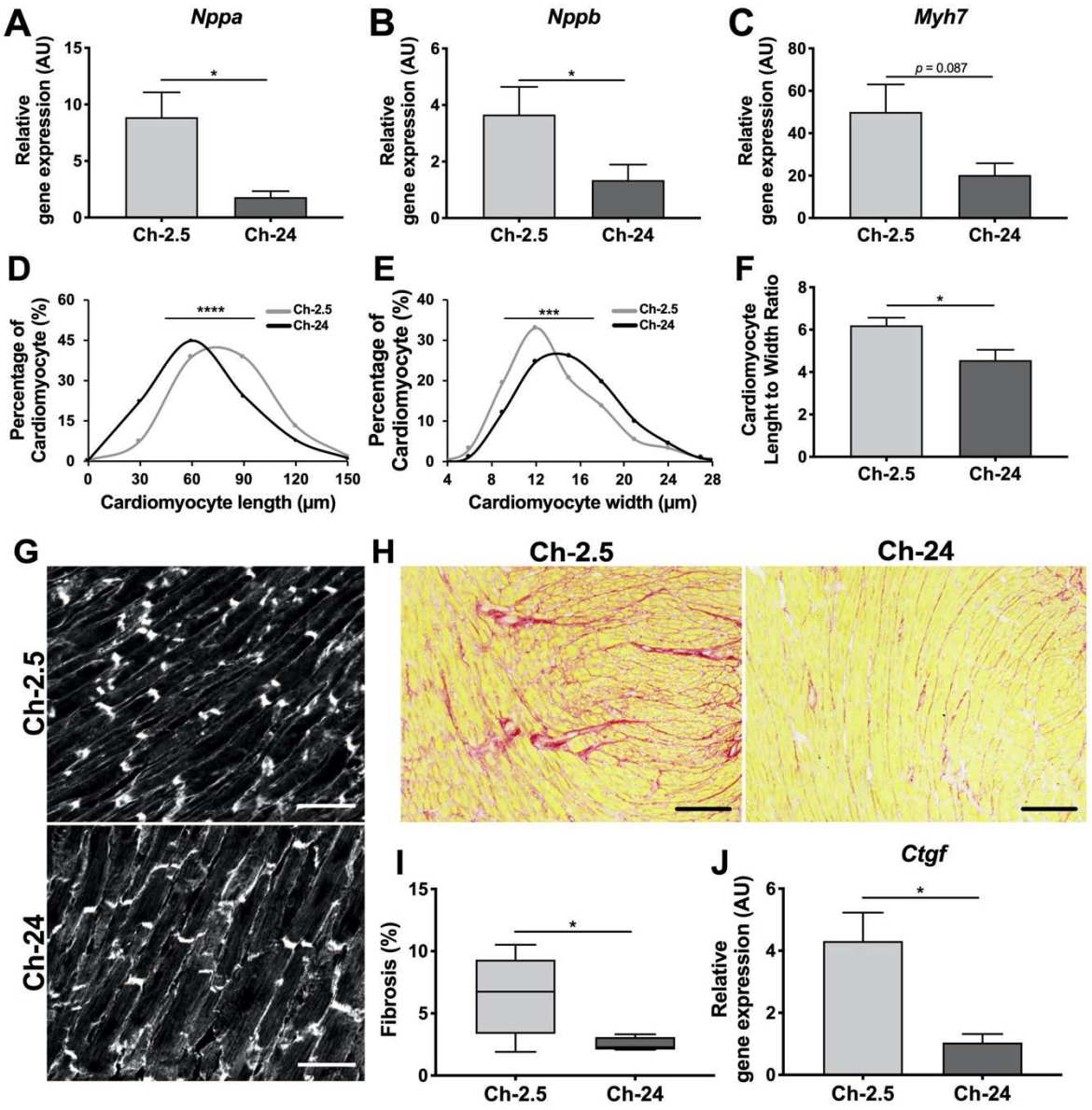

Figure 8. Impact of the Ch-24 hydrogel on cardiac remodeling after epicardial implantation in a mouse model of dilated cardiomyopathy. (A-C) Relative quantification of mRNA levels by real-time PCR for some stress-induced genes (n=7–10 per group). *Nppa*, atrial natriuretic factor (A); *Nppb*, brain natriuretic peptide (B); *Myh7*, beta-myosin heavy chain genes (C). (D-G) Morphometric analysis of cardiomyocytes after vinculin immunostaining. Distribution of cardiomyocyte lengths (D) and widths (E) in Ch-2.5 and Ch-24 hydrogels treated hearts (n>500 cardiomyocytes for each group, including five to eight mice per group). (F) Length-to-width ratio of Ch-2.5 and Ch-24 hydrogels. (G) Representative images of vinculin immunostaining of a heart section three weeks after implantation. Scale bar: 50 µm. (H-J) Assessment of cardiac fibrosis by Sirius red staining (n=5-8 per group) and by real-time PCR (n=7–10 per group). (H) Representative images of Sirius red staining of a heart section three weeks after implantation. Scale bar: 150 µm. (I) Fibrosis is expressed as the ratio (%) of the area of fibrosis to the whole area of the left ventricle. The boxes represent the lower to upper quartile range, the error bars represent the entire range, the horizontal bar represents the median value and the dot points represent mean values. (J) Relative quantification by real-time PCR of the mRNA level of a surrogate fibrosis marker, connective tissue growth factor (Ctgf). *p<0.05; **p<0.01; ***p<0.001; ****p<0.0001.

4. Discussion

The main result of this study is that the epicardial implantation of an acellular chitosan hydrogel, dependent on the DA of the chitosan, improves the functional outcomes of both ischemic and nonischemic hearts and that this benefit is associated with a significant reduction in fibrosis and hypertrophic stress.

In this study, ischemic cardiomyopathy was induced by permanent coronary ligation in rats, which is a commonly used and excellent ischemic model. One of the limits of this model lies in the differences in the observed phenotypes relative to those observed in patients, especially in the early stage, because in patients, ischemic heart disease progresses slowly, while in this model, after the permanent coronary ligation, the death of the cardiomyocytes is immediate and massive. After this early stage, it takes approximately 10 days for the infarcted area to evolve towards a predominantly fibrotic scar, and the cardiac remodeling follows a similar process compared to that observed in humans [55]. To overcome this limitation and to use a more clinically relevant animal model, we chose to implant the chitosan hydrogels 4 weeks after coronary ligation. This chronic ischemic model allowed us to explore the impact of chitosan hydrogels at the late stage of cardiac remodeling.

For the nonischemic model, we used a well-characterized and well-documented mouse model of dilated cardiomyopathy based on cardiac-specific and tamoxifen-inducible invalidation of SRF (SRF^{HKO} mice) [9,44,56,57]. As previously described, as early as 5 days after tamoxifen injection, there is a marked decrease in SRF accompanied by a progressive impairment of cardiac function, ending in dilated cardiomyopathy, heart failure, and death within 8 weeks. One of the major strengths of this model is the advantage of a timely controlled onset of functional deterioration (once tamoxifen has been given) and the reproducibility of the observed phenotypes between each individual, thereby allowing for a standardized comparison of outcomes between treated and nontreated mutant animals. Using this model, we evaluated the impact of epicardial implantation of chitosan hydrogels on adaptive cardiac remodeling. For this reason, we implanted chitosan hydrogels just after tamoxifen injection, before the onset of the dilated cardiomyopathy, and we assessed the progression of the disease over time.

Chitosan hydrogels are well-tolerated by the host myocardium after implantation, both in ischemic and nonischemic animal models. They provide structural support for the damaged ventricle and induce adaptive tissue remodeling and endogenous repair mechanisms. Chitosan is a polysaccharide classified by the United States Food and Drug Administration as a “safe” substance [58]. Chitosan-based biomaterials are widely used for tissue regeneration purposes [59]. The DA of chitosan is a key structural parameter impacting its degradation and biological activity [37,42,60,61]. However, limited data are available on the impact of the DA of the chitosan on tissue regeneration. Therefore, in this study, four different DAs ranging from 2.5% to 38% were investigated. Our results showed that

epicardial implantation of chitosan hydrogels with a DA of 24% improved the functional outcomes of both ischemic and nonischemic hearts and this benefit was associated with a significant reduction in fibrosis and hypertrophic stress. Although chitosan has been shown to modulate the immune response [24–26], interestingly, in our study, the expression of CD206, a marker of activated macrophages, and the level of cytokines measured by cytokine arrays and quantitative real-time PCR, were not modified by the chitosan treatment, suggesting that the positive effect of chitosan on the cardiac remodeling was independent of inflammation, thus implying a different scenario as described in [62]. One of the explanations for the positive effect of the Ch-24 hydrogel on cardiac function could be linked to the capacity of the chitosan patch to provide mechanical support to the injured cardiac tissue [13–16]. Although all hydrogel patches used here offer mechanical support to injured tissue regardless of the degree of acetylation, the Ch-24 hydrogel is perhaps the most suitable patch in terms of its mechanical properties (this kind of patch was not too rigid, but not too flexible either). In other hand, label-free proteomic analysis performed in the Ch-24 hydrogel treated hearts highlighted an increased expression of mitochondrial proteins and cytosolic proteins involved in the glycolysis process. These results could indicate that the treatment with the Ch-24 hydrogel was inducing a metabolic switch towards glycolysis to the detriment of the tricarboxylic acid cycle and fatty acid oxidation, which is in relation with energy preservation in the context of heart failure. These results are consistent with previous works that have shown that chitosan and their derivatives could have anti-oxidant effects [63]. It is possible that the hydrogel via the delivery of gel degradation products, depending on its degradation kinetics, protects surrounding host cardiomyocytes via induction of adaptive tissue remodeling. However, the role of chitosan gel “fragments” with different DAs in the implanted region still needs to be elucidated. Indeed, chitosan oligosaccharides exhibited a beneficial effect on cardiac cells in response to the apoptosis and oxidative stress induced by doxorubicin [64].

In accordance with the efficacy of chitosan hydrogels implantation, we observed a reduced LV wall stress in the animals treated with the Ch-24 hydrogel. Our results demonstrated the reduced expression of pro-hypertrophic stress and fibrosis markers and higher expression of cytoskeletal proteins, such as troponin I and desmin, with Ch-24 hydrogel treatment. Moreover, using a nonischemic SRF^{HKO} mouse model, we have demonstrated that the cardiomyocyte length to width ratio was significantly lower in Ch-24 hydrogel treated mice compared to Ch-2.5 hydrogel treated mice, indicating that Ch-24 hydrogel treatment prevents cardiac remodeling.

5. Conclusions

Taken together, in this study, we showed that the epicardial implantation of acellular chitosan hydrogels with a DA of 24% is able to reverse the deleterious cardiac remodeling in the setting of both ischemic and nonischemic cardiomyopathies. The extent of fibrosis, the cardiomyocyte length-to-width ratio, as well as the genes involved in fibrosis and hypertrophic stress were repressed after implantation. Our findings indicate they have great potential as a reliable therapeutic approach to heart

failure. The possibility of enriching these hydrogel patches with molecules of beneficial interest for cardiac regeneration and functional recovery of the heart is currently under study.

Funding

This work was supported by funds from Sorbonne Université, Claude Bernard Lyon 1, the CNRS, the INSERM, the Agence Nationale de la Recherche (ANR-16-CE29-0021-MYOCHITO), the Fondation de l'Avenir (grant number AP-RM-17-032), the Fédération Française de Cardiologie, Fondation France. Orianne Domengé was supported by a Ph.D. fellowship from the Agence Nationale de la Recherche (ANR-16-CE29-0021-MYOCHITO).

Conflicts of interest

N/A

CRediT authorship contribution statement

Orianne Domengé: Conceptualization, Methodology, Writing – original draft; **Hélène Ragot:** Conceptualization, Methodology, Writing – original draft; **Robin Deloux:** Conceptualization, Methodology, Writing - review & editing; **Agnès Crépet:** Methodology, Visualization; **Gaëlle Revet:** Methodology, Visualization; **Solène Emmanuelle Boitard**: Methodology, Visualization; **Alexandre Simon**: Methodology, Visualization; **Nathalie Mougenot**: Methodology, Visualization; **Laurent David**: Conceptualization, Writing - Review & Editing; **Thierry Delair**: Conceptualization, Writing - Review & Editing; **Alexandra Montembault**: Supervision, Funding acquisition, Conceptualization, Validation, Writing - Original Draft; **Onnik Agbulut**: Supervision, Funding acquisition, Conceptualization, Validation, Writing - Original Draft.

Acknowledgments

The authors thank Lea Deltourbe, Christina Fissoun, Zakaria Mougin, Lucas Rougier, Ceren Yazici (IBPS, Paris-France) and Maria Mihoc (UMS28, Paris-France) for punctual technical assistance. The authors also thank all of the personnel of the Animal Facility of the Sorbonne Université (UMS28, Paris-France); the Microscopy Platform (IBPS, Paris-France) for helpful advice and technical assistance during microscopy image acquisition and analysis; and the Proteomics facility (Jacques Monod Institute, Paris-France) for performing the mass spectrometry experiments and for their support in data analysis.

Bibliography

[1] D. Tomasoni, M. Adamo, C.M. Lombardi, M. Metra, Highlights in heart failure, ESC Heart Fail. 6 (2019) 1105–1127. https://doi.org/10.1002/ehf2.12555.

[2] A.L. Bui, T.B. Horwich, G.C. Fonarow, Epidemiology and risk profile of heart failure, Nat. Rev. Cardiol. 8 (2011) 30–41. https://doi.org/10.1038/nrcardio.2010.165.

[3] N.T. Feric, M. Radisic, Strategies and Challenges to Myocardial Replacement Therapy, Stem Cells Transl. Med. 5 (2016) 410–416. https://doi.org/10.5966/sctm.2015-0288.

[4] M. Kitsara, O. Agbulut, D. Kontziampasis, Y. Chen, P. Menasché, Fibers for hearts: A critical review on electrospinning for cardiac tissue engineering, Acta Biomater. 48 (2017) 20–40. https://doi.org/10.1016/j.actbio.2016.11.014.

[5] C.P. Jackman, A.M. Ganapathi, H. Asfour, Y. Qian, B.W. Allen, Y. Li, N. Bursac, Engineered cardiac tissue patch maintains structural and electrical properties after epicardial implantation, Biomaterials. 159 (2018) 48–58. https://doi.org/10.1016/j.biomaterials.2018.01.002.

[6] L. Ye, W.-H. Zimmermann, D.J. Garry, J. Zhang, Patching the heart: cardiac repair from within and outside, Circ. Res. 113 (2013) 922–932. https://doi.org/10.1161/CIRCRESAHA.113.300216.

[7] H. Hamdi, A. Furuta, V. Bellamy, A. Bel, E. Puymirat, S. Peyrard, O. Agbulut, P. Menasché, Cell delivery: intramyocardial injections or epicardial deposition? A head-to-head comparison, Ann. Thorac. Surg. 87 (2009) 1196–1203. https://doi.org/10.1016/j.athoracsur.2008.12.074.

[8] H. Hamdi, V. Planat-Benard, A. Bel, E. Puymirat, R. Geha, L. Pidial, H. Nematalla, V. Bellamy, P. Bouaziz, S. Peyrard, L. Casteilla, P. Bruneval, A.A. Hagège, O. Agbulut, P. Menasché, Epicardial adipose stem cell sheets results in greater post-infarction survival than intramyocardial injections, Cardiovasc. Res. 91 (2011) 483–491. https://doi.org/10.1093/cvr/cvr099.

[9] H. Hamdi, S. Boitard, V. Planat-Benard, J. Pouly, H. Neamatalla, P. Joanne, M.-C. Perier, V. Bellamy, L. Casteilla, Z. Li, A. Hagège, M. Mericskay, P. Menasché, O. Agbulut, Efficacy of Epicardially-delivered Adipose Stroma Cell Sheets in Dilated Cardiomyopathy, Cardiovasc. Res. (2013). https://doi.org/10.1093/cvr/cvt149.

[10] J.A. Burdick, R.L. Mauck, J.H. Gorman, R.C. Gorman, Acellular biomaterials: an evolving alternative to cell-based therapies, Sci. Transl. Med. 5 (2013) 176ps4. https://doi.org/10.1126/scitranslmed.3003997.

[11] D.A. Svystonyuk, H.E.M. Mewhort, P.W.M. Fedak, Using Acellular Bioactive Extracellular Matrix Scaffolds to Enhance Endogenous Cardiac Repair, Front. Cardiovasc. Med. 5 (2018) 35. https://doi.org/10.3389/fcvm.2018.00035.

[12] J.L. Dziki, B.M. Sicari, M.T. Wolf, M.C. Cramer, S.F. Badylak, Immunomodulation and Mobilization of Progenitor Cells by Extracellular Matrix Bioscaffolds for Volumetric Muscle Loss Treatment, Tissue Eng. Part A. 22 (2016) 1129–1139. https://doi.org/10.1089/ten.TEA.2016.0340.

[13] V. Serpooshan, M. Zhao, S.A. Metzler, K. Wei, P.B. Shah, A. Wang, M. Mahmoudi, A.V. Malkovskiy, J. Rajadas, M.J. Butte, D. Bernstein, P. Ruiz-Lozano, The effect of bioengineered

acellular collagen patch on cardiac remodeling and ventricular function post myocardial infarction, Biomaterials. 34 (2013) 9048–9055. https://doi.org/10.1016/j.biomaterials.2013.08.017.

[14] H.E.M. Mewhort, J.D. Turnbull, A. Satriano, K. Chow, J.A. Flewitt, A.-C. Andrei, D.G. Guzzardi, D.A. Svystonyuk, J.A. White, P.W.M. Fedak, Epicardial infarct repair with bioinductive extracellular matrix promotes vasculogenesis and myocardial recovery, J. Heart Lung Transplant. Off. Publ. Int. Soc. Heart Transplant. 35 (2016) 661–670. https://doi.org/10.1016/j.healun.2016.01.012.

[15] Y. Efraim, H. Sarig, N. Cohen Anavy, U. Sarig, E. de Berardinis, S.-Y. Chaw, M. Krishnamoorthi, J. Kalifa, H. Bogireddi, T.V. Duc, T. Kofidis, L. Baruch, F.Y.C. Boey, S.S. Venkatraman, M. Machluf, Biohybrid cardiac ECM-based hydrogels improve long term cardiac function post myocardial infarction, Acta Biomater. 50 (2017) 220–233. https://doi.org/10.1016/j.actbio.2016.12.015.

[16] D.S.J. Park, H.E.M. Mewhort, G. Teng, D. Belke, J. Turnbull, D. Svystonyuk, D. Guzzardi, S. Kang, P.W.M. Fedak, Heparin Augmentation Enhances Bioactive Properties of Acellular Extracellular Matrix Scaffold, Tissue Eng. Part A. 24 (2018) 128–134. https://doi.org/10.1089/ten.TEA.2017.0004.

[17] G.H. Kim, N. Uriel, D. Burkhoff, Reverse remodelling and myocardial recovery in heart failure, Nat. Rev. Cardiol. 15 (2018) 83–96. https://doi.org/10.1038/nrcardio.2017.139.

[18] Y. Han, W. Yang, W. Cui, K. Yang, X. Wang, Y. Chen, L. Deng, Y. Zhao, W. Jin, Development of functional hydrogels for heart failure, J. Mater. Chem. B. 7 (2019) 1563–1580. https://doi.org/10.1039/C8TB02591F.

[19] M.W. Tibbitt, K.S. Anseth, Hydrogels as extracellular matrix mimics for 3D cell culture, Biotechnol. Bioeng. 103 (2009) 655–663. https://doi.org/10.1002/bit.22361.

[20] H. Geckil, F. Xu, X. Zhang, S. Moon, U. Demirci, Engineering hydrogels as extracellular matrix mimics, Nanomed. 5 (2010) 469–484. https://doi.org/10.2217/nnm.10.12.

[21] L.T. Saldin, M.C. Cramer, S.S. Velankar, L.J. White, S.F. Badylak, Extracellular matrix hydrogels from decellularized tissues: Structure and function, Acta Biomater. 49 (2017) 1–15. https://doi.org/10.1016/j.actbio.2016.11.068.

[22] A.J. Rufaihah, D. Seliktar, Hydrogels for therapeutic cardiovascular angiogenesis, Adv. Drug Deliv. Rev. 96 (2016) 31–39. https://doi.org/10.1016/j.addr.2015.07.003.

[23] C. Chatelet, O. Damour, A. Domard, Influence of the degree of acetylation on some biological properties of chitosan films, Biomaterials. 22 (2001) 261–268. https://doi.org/10.1016/s0142-9612(00)00183-6.

[24] Y. Zhao, Y. Wang, J. Gong, L. Yang, C. Niu, X. Ni, Y. Wang, S. Peng, X. Gu, C. Sun, Y. Yang, Chitosan degradation products facilitate peripheral nerve regeneration by improving macrophage-constructed microenvironments, Biomaterials. 134 (2017) 64–77. https://doi.org/10.1016/j.biomaterials.2017.02.026.

[25] S.-H. Chang, Y.-Y. Lin, G.-J. Wu, C.-H. Huang, G.J. Tsai, Effect of chitosan molecular weight on anti-inflammatory activity in the RAW 264.7 macrophage model, Int. J. Biol. Macromol. 131 (2019) 167–175. https://doi.org/10.1016/j.ijbiomac.2019.02.066.

[26] J. Chedly, S. Soares, A. Montembault, Y. von Boxberg, M. Veron-Ravaille, C. Mouffle, M.-N.

Benassy, J. Taxi, L. David, F. Nothias, Physical chitosan microhydrogels as scaffolds for spinal cord injury restoration and axon regeneration, Biomaterials. 138 (2017) 91–107. https://doi.org/10.1016/j.biomaterials.2017.05.024.

[27] M. Kong, X.G. Chen, K. Xing, H.J. Park, Antimicrobial properties of chitosan and mode of action: a state of the art review, Int. J. Food Microbiol. 144 (2010) 51–63. https://doi.org/10.1016/j.ijfoodmicro.2010.09.012.

[28] E. Khor, L.Y. Lim, Implantable applications of chitin and chitosan, Biomaterials. 24 (2003) 2339–2349. https://doi.org/10.1016/s0142-9612(03)00026-7.

[29] M. Ishihara, K. Ono, M. Sato, K. Nakanishi, Y. Saito, H. Yura, T. Matsui, H. Hattori, M. Fujita, M. Kikuchi, A. Kurita, Acceleration of wound contraction and healing with a photocrosslinkable chitosan hydrogel, Wound Repair Regen. Off. Publ. Wound Heal. Soc. Eur. Tissue Repair Soc. 9 (2001) 513–521. https://doi.org/10.1046/j.1524-475x.2001.00513.x.

[30] K. Ono, M. Ishihara, Y. Ozeki, H. Deguchi, M. Sato, Y. Saito, H. Yura, M. Sato, M. Kikuchi, A. Kurita, T. Maehara, Experimental evaluation of photocrosslinkable chitosan as a biologic adhesive with surgical applications, Surgery. 130 (2001) 844–850. https://doi.org/10.1067/msy.2001.117197.

[31] G. Lamarque, M. Cretenet, C. Viton, A. Domard, New route of deacetylation of alpha- and beta-chitins by means of freeze--pump out--thaw cycles, Biomacromolecules. 6 (2005) 1380–1388. https://doi.org/10.1021/bm049322b.

[32] J.A. de M. Delezuk, M.B. Cardoso, A. Domard, S.P. Campana-Filho, Ultrasound-assisted deacetylation of beta-chitin: influence of processing parameters, Polym. Int. 60 (2011) 903–909. https://doi.org/10.1002/pi.3037.

[33] A. Domard, A perspective on 30 years research on chitin and chitosan, Carbohydr. Polym. 84 (2011) 696–703. https://doi.org/10.1016/j.carbpol.2010.04.083.

[34] C. Schatz, C. Viton, T. Delair, C. Pichot, A. Domard, Typical physicochemical behaviors of chitosan in aqueous solution, Biomacromolecules. 4 (2003) 641–648. https://doi.org/10.1021/bm025724c.

[35] P. Sorlier, A. Denuzière, C. Viton, A. Domard, Relation between the degree of acetylation and the electrostatic properties of chitin and chitosan, Biomacromolecules. 2 (2001) 765–772. https://doi.org/10.1021/bm015531+.

[36] A. Montembault, C. Viton, A. Domard, Rheometric study of the gelation of chitosan in aqueous solution without cross-linking agent, Biomacromolecules. 6 (2005) 653–662. https://doi.org/10.1021/bm049593m.

[37] L. Rami, S. Malaise, S. Delmond, J.-C. Fricain, R. Siadous, S. Schlaubitz, E. Laurichesse, J. Amédée, A. Montembault, L. David, L. Bordenave, Physicochemical modulation of chitosan-based hydrogels induces different biological responses: interest for tissue engineering, J. Biomed. Mater. Res. A. 102 (2014) 3666–3676. https://doi.org/10.1002/jbm.a.35035.

[38] K.I. Draget, K.M. Vårum, E. Moen, H. Gynnild, O. Smidsrød, Chitosan cross-linked with Mo(VI) polyoxyanions: a new gelling system, Biomaterials. 13 (1992) 635–638. https://doi.org/10.1016/0142-9612(92)90032-j.

[39] L. Vachoud, N. Zydowicz, A. Domard, Formation and characterisation of a physical chitin gel, Carbohydr. Res. 302 (1997) 169–177. https://doi.org/10.1016/S0008-6215(97)00126-2.

[40] A. Montembault, C. Viton, A. Domard, Physico-chemical studies of the gelation of chitosan in a hydroalcoholic medium, Biomaterials. 26 (2005) 933–943. https://doi.org/10.1016/j.biomaterials.2004.03.033.

[41] A. Fiamingo, A. Montembault, S.-E. Boitard, H. Naemetalla, O. Agbulut, T. Delair, S.P. Campana-Filho, P. Menasché, L. David, Chitosan Hydrogels for the Regeneration of Infarcted Myocardium: Preparation, Physicochemical Characterization, and Biological Evaluation, Biomacromolecules. 17 (2016) 1662–1672. https://doi.org/10.1021/acs.biomac.6b00075.

[42] S. Malaise, L. Rami, A. Montembault, P. Alcouffe, B. Burdin, L. Bordenave, S. Delmond, L. David, Bioresorption mechanisms of chitosan physical hydrogels: a scanning electron microscopy study, Mater. Sci. Eng. C Mater. Biol. Appl. 42 (2014) 374–384. https://doi.org/10.1016/j.msec.2014.04.060.

[43] A. Hirai, H. Odani, A. Nakajima, Determination of degree of deacetylation of chitosan by 1H NMR spectroscopy, Polym. Bull. 26 (1991) 87–94. https://doi.org/10.1007/BF00299352.

[44] A. Parlakian, C. Charvet, B. Escoubet, M. Mericskay, J.D. Molkentin, G. Gary-Bobo, L.J. De Windt, M.-A. Ludosky, D. Paulin, D. Daegelen, D. Tuil, Z. Li, Temporally controlled onset of dilated cardiomyopathy through disruption of the SRF gene in adult heart, Circulation. 112 (2005) 2930–2939. https://doi.org/10.1161/CIRCULATIONAHA.105.533778.

[45] H. Hamdi, V. Planat-Benard, A. Bel, H. Neamatalla, L. Saccenti, D. Calderon, V. Bellamy, M. Bon, M.-C. Perrier, C. Mandet, P. Bruneval, L. Casteilla, A.A. Hagège, M. Pucéat, O. Agbulut, P. Menasché, Long-term functional benefits of epicardial patches as cell carriers, Cell Transplant. 23 (2014) 87–96. https://doi.org/10.3727/096368912X658836.

[46] V. Bellamy, V. Vanneaux, A. Bel, H. Nemetalla, S. Emmanuelle Boitard, Y. Farouz, P. Joanne, M.-C. Perier, E. Robidel, C. Mandet, A. Hagège, P. Bruneval, J. Larghero, O. Agbulut, P. Menasché, Long-term functional benefits of human embryonic stem cell-derived cardiac progenitors embedded into a fibrin scaffold, J. Heart Lung Transplant. Off. Publ. Int. Soc. Heart Transplant. 34 (2015) 1198–1207. https://doi.org/10.1016/j.healun.2014.10.008.

[47] S. Popa-Nita, C. Rochas, L. David, A. Domard, Structure of natural polyelectrolyte solutions: role of the hydrophilic/hydrophobic interaction balance, Langmuir ACS J. Surf. Colloids. 25 (2009) 6460–6468. https://doi.org/10.1021/la900061n.

[48] S. Popa-Nita, P. Alcouffe, C. Rochas, L. David, A. Domard, Continuum of structural organization from chitosan solutions to derived physical forms, Biomacromolecules. 11 (2010) 6–12. https://doi.org/10.1021/bm9012138.

[49] N. Sereni, A. Enache, G. Sudre, A. Montembault, C. Rochas, P. Durand, M.-H. Perrard, G. Bozga, J.-P. Puaux, T. Delair, L. David, Dynamic Structuration of Physical Chitosan Hydrogels, Langmuir ACS J. Surf. Colloids. 33 (2017) 12697–12707. https://doi.org/10.1021/acs.langmuir.7b02997.

[50] K. Almdal, J. Dyre, S. Hvidt, O. Kramer, Towards a phenomenological definition of the term ‘gel,’ Polym. Gels Netw. 1 (1993) 5–17. https://doi.org/10.1016/0966-7822(93)90020-I.

[51] S.B. Ross-Murphy, H. McEvoy, Fundamentals of Hydrogels and Gelation, Br. Polym. J. 18 (1986) 2–7. https://doi.org/10.1002/pi.4980180103.

[52] A.H. Clark, S.B. Ross-Murphy, Structural and mechanical properties of biopolymer gels, in: Biopolymers, Springer, Berlin, Heidelberg, 1987: pp. 57–192. https://doi.org/10.1007/BFb0023332.

[53] M. Shiraishi, Y. Shintani, Y. Shintani, H. Ishida, R. Saba, A. Yamaguchi, H. Adachi, K. Yashiro, K. Suzuki, Alternatively activated macrophages determine repair of the infarcted adult murine heart, J. Clin. Invest. 126 (2016) 2151–2166. https://doi.org/10.1172/JCI85782.

[54] W.H. Gaasch, Left ventricular radius to wall thickness ratio, Am. J. Cardiol. 43 (1979) 1189–1194. https://doi.org/10.1016/0002-9149(79)90152-8.

[55] B.I. Jugdutt, M.J. Joljart, M.I. Khan, Rate of collagen deposition during healing and ventricular remodeling after myocardial infarction in rat and dog models, Circulation. 94 (1996) 94–101. https://doi.org/10.1161/01.cir.94.1.94.

[56] R. Deloux, D. Vitiello, N. Mougenot, P. Noirez, Z. Li, M. Mericskay, A. Ferry, O. Agbulut, Voluntary Exercise Improves Cardiac Function and Prevents Cardiac Remodeling in a Mouse Model of Dilated Cardiomyopathy, Front. Physiol. 8 (2017) 899. https://doi.org/10.3389/fphys.2017.00899.

[57] P. Joanne, M. Kitsara, S.-E. Boitard, H. Naemetalla, V. Vanneaux, M. Pernot, J. Larghero, P. Forest, Y. Chen, P. Menasché, O. Agbulut, Nanofibrous clinical-grade collagen scaffolds seeded with human cardiomyocytes induces cardiac remodeling in dilated cardiomyopathy, Biomaterials. 80 (2016) 157–168. https://doi.org/10.1016/j.biomaterials.2015.11.035.

[58] P. Baldrick, The safety of chitosan as a pharmaceutical excipient, Regul. Toxicol. Pharmacol. RTP. 56 (2010) 290–299. https://doi.org/10.1016/j.yrtph.2009.09.015.

[59] R.C.F. Cheung, T.B. Ng, J.H. Wong, W.Y. Chan, Chitosan: An Update on Potential Biomedical and Pharmaceutical Applications, Mar. Drugs. 13 (2015) 5156–5186. https://doi.org/10.3390/md13085156.

[60] A. Montembault, K. Tahiri, C. Korwin-Zmijowska, X. Chevalier, M.-T. Corvol, A. Domard, A material decoy of biological media based on chitosan physical hydrogels: application to cartilage tissue engineering, Biochimie. 88 (2006) 551–564. https://doi.org/10.1016/j.biochi.2006.03.002.

[61] F. Croisier, C. Jérôme, Chitosan-based biomaterials for tissue engineering, Eur. Polym. J. 49 (2013) 780–792. https://doi.org/10.1016/j.eurpolymj.2012.12.009.

[62] A. Hanna, N.G. Frangogiannis, The Role of the TGF-β Superfamily in Myocardial Infarction, Front. Cardiovasc. Med. 6 (2019) 140. https://doi.org/10.3389/fcvm.2019.00140.

[63] V.P. Varlamov, A.V. Il'ina, B.Ts. Shagdarova, A.P. Lunkov, I.S. Mysyakina, Chitin/Chitosan and Its Derivatives: Fundamental Problems and Practical Approaches, Biochem. Mosc. 85 (2020) 154–176. https://doi.org/10.1134/S0006297920140084.

[64] Y. Zhang, K.A. Ahmad, F.U. Khan, S. Yan, A.U. Ihsan, Q. Ding, Chitosan oligosaccharides prevent doxorubicin-induced oxidative stress and cardiac apoptosis through activating p38 and JNK MAPK mediated Nrf2/ARE pathway, Chem. Biol. Interact. 305 (2019) 54–65. https://doi.org/10.1016/j.cbi.2019.03.027.

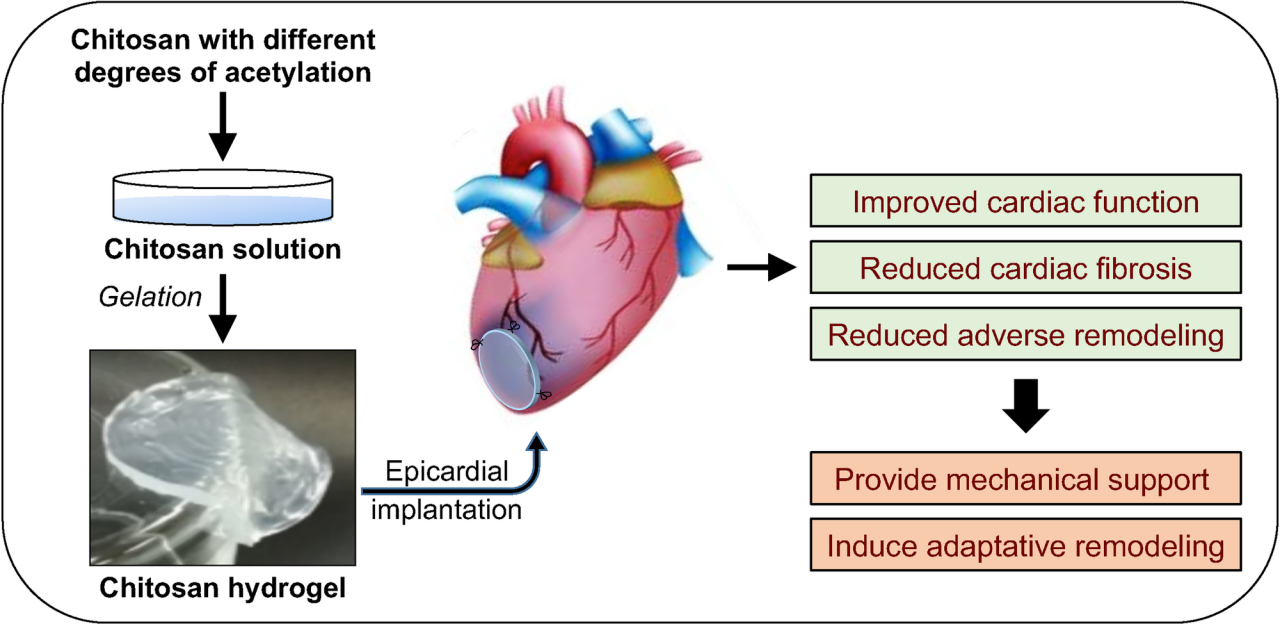
Chitosan with different degrees of acetylation
Chitosan solution
Gelation
Chitosan hydrogel
Epicardial implantation
Improved cardiac function
Reduced cardiac fibrosis
Reduced adverse remodeling
Provide mechanical support
Induce adaptative remodeling